DISSERTATIONES
TECHNOLOGIAE
UNIVERSITATIS
TARTUENSIS
32

VEIKO VUNDER

Modeling and characterization of back-relaxation of ionic electroactive polymer actuators

DISSERTATIONES TECHNOLOGIAE UNIVERSITATIS TARTUENSIS
32

VEIKO VUNDER

Modeling and characterization of back-relaxation of ionic electroactive polymer actuators

UNIVERSITY OF TARTU
Press

This study was carried out at the Institute of Technology, Faculty of Science and Technology, University of Tartu, Estonia.

The dissertation was admitted on June 22, 2016 in partial fulfillment of the requirements for the degree of Doctor of Philosophy (Physical Engineering) and allowed for defense by the Scientific Council of the Institute of Technology of the Faculty of Science and Technology of the University of Tartu.

Supervisors: Dr. Andres Punning, University of Tartu
Prof. Alvo Aabloo, University of Tartu

Opponent: Prof. Barbar Akle, Lebanese American University School of Engineering, Department of Industrial & Mechanical Engineering, Lebanon

Defense: Auditorium 121, Nooruse 1, Tartu, Estonia on August 22, 2016 at 14:00

Publication of this thesis is granted by the Institute of Technology, Faculty of Science and Technology, University of Tartu.

ISSN 2228-0855
ISBN 978-9949-77-183-7 (print)
ISBN 978-9949-77-184-4 (pdf)

University of Tartu Press
www.tyk.ee

CONTENTS

LIST OF ORIGINAL PUBLICATIONS

I. Vunder, V., Punning, A., and Aabloo, A. (2012) **Mechanical interpretation of back-relaxation of ionic electroactive polymer actuators**, Smart Materials & Structures, **21**(11), 115023.

II. Vunder, V., Punning, A., and Aabloo, A. (2012) **Back-relaxation of carbon-based ionic electroactive polymer actuators**, ASME 2012 Conference on Smart Materials, Adaptive Structures and Intelligent Systems. ASME, 163–168.

III. Vunder, V., Punning, A., and Aabloo, A. (2015) **Electromechanical distributed modeling of ionic polymer metal composites**, Ionic Polymer Metal Composites (IPMCs): Smart Multi-Functional Materials and Artificial Muscles, **1**, 228–247

IV. Vunder, V., Punning, A., and Aabloo, A. (2013). **Viscoelastic model of IPMC actuators**, Proceedings of SPIE, 868723.

V. Vunder, V., Hamburg, E., Johanson, U., Punning, A., and Aabloo, A. (2016) **Effect of ambient humidity on ionic electroactive polymer actuators**, Smart Materials & Structures, **25**(5), 055038

VI. Punning, A., Vunder, V., Must, I., Johanson, U., Anbarjafari, G., and Aabloo, A. (2016) ***In situ* scanning electron microscopy study of strains of ionic electroactive polymer actuators**, Journal of Intelligent Material Systems and Structures, **27**(8), 1061–1074

Author's contribution

In papers I–IV, author conducted all experiments including preparing the experimental setups and programming necessary software. The author analyzed all the acquired data, developed models, performed simulations, and was responsible for writing the papers.

The author's contribution to paper V were conducting the electrical and electromechanical measurements, analyzing the data, developing and simulating the models, and writing the paper.

In paper VI, the author developed the MATLAB scripts of the digital image correlation method to fit the requirements of processing the SEM images, calculating the strains, bending moments, beam energies, etc.

Other related publications

- Vunder, V., Itik, M., Põldsalu, I., Punning, A., and Aabloo, A. (2014) **Inversion-based control of ionic polymer–metal composite actuators with nanoporous carbon-based electrodes**, Smart Materials and Structures, **23**(2), 025010.
- Vunder, V., Punning, A., Aabloo, A. (2015). **Long-term behavior of ionic electroactive polymer actuators in variable humidity conditions**, Proceedings of SPIE, 90561Y

LIST OF ABBREVIATIONS

(in alphabetical order)

BMIm	1-butyl-3-methylimidazolium (cation)
CDC	carbide derived carbon
CNT	carbon nanotube
CP	conductive polymer
DAP	direct assembly process
DE	differential evolution (fitting method)
DMA	dynamical mechanical analysis
EAP	electroactive polymer
EDLC	electric double layer capacitor
EDL	electric double layer
EMIm	1-ethyl-3-methylimidazolium (cation)
IEAP	ionic electroactive polymer
IL	ionic liquid (narrowed in this thesis to room temperature ionic liquid)
IPMC	ionic polymer–metal composite
MWCNT	multi-walled carbon nanotube
NMR	nuclear magnetic resonance
PC	4-methyl-1,3-dioxolan-2-one, propylene carbonate
PDE	partial differential equation
PFG NMR	pulsed field gradient nuclear magnetic resonance
PVdF	polyvinylidene fluoride
PVdF(HFP)	polyvinylidene fluoride-co-hexafluoropropylene
RH	relative humidity
SWCNT	single-walled carbon nanotube
TBA	tetrabutylammonium (cation)
TMA	tetramethylammonium (cation)
TFS	trifluoromethanesulfonate (anion)
TFSI	bis(trifluoromethanesulfonyl)imide (anion)

1. INTRODUCTION

The significance of smart materials in modern devices and systems has rapidly increased during the past two decades. The material is considered "smart" if it is coupled between multiple physical domains, for example, converts electrical signals to mechanical deformation (actuator) or converts mechanical deformation to electrical signals (sensor or energy harvester) [1]. Those materials are especially desired in the fields of robotics where flexible circuits and soft manipulators incorporated with sensory arrays are of interest. Smart materials can be integrated into bioinspired robots, medical devices, tactile displays, microelectromechanical systems (MEMS), lab-on-chip systems, to name a few.

Most of the industrial robots consist of joined rigid parts, which are often complicated and which are unreasonably expensive or even impossible to miniaturize. In nature, on the contrary, the vast majority of the biological structures are flexible and able to generate motion without motors, gears, and other rigid mechanical constituents. Hence, it is of great interest of scientists to replicate these already optimized flexible structures and mimic their behavior (for example, swimming fish, flying bat, etc.). The overall goal is to perform advanced manipulation and sensing in an efficient, simple, and more natural way.

To date, virtually in all fields of technologies conventional materials, such as metals and metal alloys, are replaced by natural or synthetic polymers. Polymers have advantages in terms of design, manufacturing techniques, and their easily customizable properties. Methods for mass-production have already been developed, making the manufacturing of polymer materials relatively inexpensive.

This dissertation focuses on a particular type of smart materials called electroactive polymers (EAPs). EAP is an active polymer material, which changes its physical or chemical properties in response to external electrical stimulus. A certain similarity between EAP materials and biological muscles exists – both are soft and respond to electrical stimulus with kinematics. That is why EAP materials are in regular basis referred as "*artificial muscles*" [2]. Nevertheless, it is important to understand that this similarity is only appropriate for the transduction between electrical and mechanical domains. While the electromechanical conversion in EAPs takes place through physical processes, such as, electrostatic forces, electroosmotic flow, or ion migration, the actual biological muscle is described by sliding filament theory [3], where the contraction is caused by interaction of myosin and actin proteins in presence of calcium ions and adenosine triphosphate (ATP) molecules. In other words, in biological muscle, the electrical nervous signals are not the source of energy. Instead, the nervous signals function only as a triggering mechanism to release the chemical energy of ATP.

A subgroup of EAP materials that contain ions and where the electrical stimulus causes ion interaction are classified as ionic electroactive polymers or IEAPs [2]. A typical IEAP consists of a porous ion-permeable polymer

membrane, covered from both sides with electronically conductive electrodes. The electrodes are made of a noble metal (usually platinum or gold), conductive polymers (CP), or some allotrope of carbon, for example, graphene, carbon black, carbon nanotubes (CNTs), carbide-derived carbon (CDC). Both, the membrane and electrode layers contain electrolyte or electrolyte solution, which ensures the ionic conductivity between the opposite electrodes and gives to the laminate its electroactive properties. Voltage applied between the electrodes makes ions of the electrolyte to migrate inside the laminate. Under favorable conditions, this may lead to bending of the laminate. There exists also the opposite effect – mechanical deformation of the laminate alters the hydrodynamic balance of cations and anions within the boundaries of the laminate. The uneven distribution of charges can be registered as an electrical signal – voltage or electric current – between the electrodes. According to that, the IEAP materials function as electromechanical actuators or mechanoelectrical sensors, or even both simultaneously. The applicability of IEAPs is certainly not limited to actuators and sensors only, but are prospective, for example, in energy storage and energy harvesting tasks.

IEAP materials have many attractive features such as simplicity, softness, resilience, lightweight, silent operation, scalability, ease of miniaturization, allowed for microfabrication, low cost, simultaneous sensing and energy storage properties, etc. Since the actuation of IEAPs is achieved using low voltage input signals, they are directly compatible with a range of consumer electronics. Other promising fields of applications, namely, bioinspired soft robotics [4], micromanipulation [5], active guiding [6] for robotic surgery [7], vibration sensing [8], active damping [9], etc., have been proposed for IEAPs.

To operate IEAPs in the applications, a precise control over the displacement or force is required. Fluent control of IEAPs, however, is hindered by several processes, such as, creep of the polymer, solvent "leakage" to lower pressure areas or even out of the material, solvent evaporation, alteration of electrode conductivity during deformation (for example, electrode cracking). In addition, ambient parameters such as atmospheric pressure, temperature, or humidity could influence the performance of IEAPs. Moreover, the IEAP system itself may become irreversibly changed if it is controlled with improper driving signals – too high electrical current causes excessive heating of the resistive parts and too high potential results in unwanted electrochemical reactions. For example, Shahinpoor [10] showed that with less than 3.0 V DC voltage, the temperature elevated about 10 °C. Punning *et al.* [11] registered temperatures of more than 85 °C while continuously driving the IEAP actuator with 3.5 V DC steps. This has a significant impact on mechanical and electrical properties of the actuator. Naturally, the limits for each particular IEAP material are depending on their constituents and on the specific environment where the device is operated in.

The very first IEAPs were designed to operate in aqueous solutions (mostly in deionized water), while the desired environment for majority of the novel IEAPs is ambient air. Taking the water-based IEAP devices to ambient air

introduces complications, such as, solvent evaporation [12,13]. Additionally, when electrochemical stability window of water (1.23 V) is exceeded, the water starts to decompose into hydrogen and oxygen gas [14]. The named difficulties instantly alter the dynamics of the actuators [15] and result in rather short lifetime [13,16]. For enhanced stability in open-air applications, the novel IEAPs compromise, for example, organic solvents (such as, ethylene glycol [17]) or nonvolatile ionic liquids (ILs) [13,16].

ILs are salts, which at relatively low temperature (<100 degrees C) are in liquid state. The scope of this dissertation concerns only ionic liquids that are in liquid state at or below room temperature (<25 °C), also referred in literature as room temperature ionic liquids (RTILs). Superior properties such as non-volatility (that is extremely low vapor pressure), high thermal stability, wide liquidus range, wide electrochemical stability window, and high ionic conductivity, make ILs desired electrolytes for many IEAPs [13,18]. It is reported that at least a million simple ILs are possible [19] offering a huge variety of tailored physical properties. Compared to other volatile organic compounds, ILs do not cause atmospheric pollution and are recognized in many publications as green and environmentally friendly solvents [20]. Even while evaporation is not an issue to be addressed, the question about recovery of the products and solvent purification remains topical.

The thesis at hand provides a distributed electromechanical model, which takes into account the back-relaxation phenomena of IEAP actuators. As the model is based on electrical equivalent circuit of IEAP, it is scalable and suits well for characterization and comparison of different type of IEAPs. Though the general aim of the thesis is to provide the model and characterize IEAP with nanoporous carbon-based electrodes, a comparison with classical water-based ionic polymer–metal composite (IPMC) is provided. Furthermore, IEAP materials with different constituents are investigated and characterized in various ambient environments.

2. IONIC ELECTROACTIVE POLYMERS

2.1. Historic overview

The beginning of IEAP actuators goes back to 1965 when Hamlen *et al.* [21] first reported on ionic polymer gels, which can be electrically controlled. In principle, polymer gel actuators contract or expand depending on the pH level of the electrolyte solution. If the solution becomes more acidic, the gel contracts. Oppositely, the solution that becomes more alkaline causes expansion of the gel. As the pH of the solution changes when applying electric field and current, the subsequent volumetric effects can be electrically controlled through altering the pH of the solution. The swelling of polymer gel actuators were mostly described in terms of linear expansion/contraction. In 1985, Osada and Hasebe [22] reported on a first water-swollen polymer gel, which was sandwiched between two electrodes made of platinum wire. They observed reversible switching (bending) between two stable states. Osada and Hasebe also combined ionic polymer gel with a rather stiff polyvinyl chloride (PVC) layer in order to obtain bending motion, identically to a bimetal beam, but driven electrically.

Prior to 1990s, many other followers, namely, De Rossi [23], Osada and Kishi [24], contributed to the evolution of ionic polymer gels. In the beginning of 1990s, Grimshaw, Nussbaum, Grodinzky, *et al.* [25] provided a model to describe the kinetics of swelling and shrinking in polyelectrolyte gels. Caldwell and Taylor [26] investigated polyelectrolyte gels and determined responses under chemical stimulus to use the muscle-like actuator in artificial muscles. Other concepts that fully exploit flexible bending functionality, for example, swimming robots [27], robotic arms [28], and distributed actuation devices [29], were suggested. Segalman *et al.* [30] discuss about the mechanisms of ionic polymer gel actuators, give corresponding mathematical formulations and suggest these actuators for space applications. In 1992, Osada, Okuzaki and Hirofumi presented worm-like polymer gel actuator that could move 25 cm per minute. The necessary electric field 10 V per cm was generated using a 20 V DC power supply.

Since the beginning of 1990s, another type of IEAP actuators – ionic polymer–metal composites (IPMCs) – have been developed. IPMC consists of a perfluorinated polymer backbone with fixed anions and mobile cations. The ion-polymer membrane is covered from both sides with metal electrodes. When an electric field between the electrodes is induced, the ion migration inside the laminate causes bending of the material. In 1989, Fedkiw and Her [31] introduced impregnation-reduction method for preparing metalized electrodes on Nafion® polymer. The currently accepted term “IPMC” was first introduced about 10 years later in 1998 by Shahinpoor *et al.* [32]. Since then, and also later in some publications, the same composite was alternatively known as Ionic Conducting Polymer gel Film or ICPF [6,29,33]. So, the credit for the conceptual design of IPMC is shared by many authors previously working with polymer gels including Shahinpoor [27], Sadeghipour [8], and Oguro [34].

The rapid development of IEAPs in the twenty-first century revealed new electrode materials, manufacturing methods, and solvents. In 1999, Baughman *et*

al. [35] demonstrated single-walled carbon nanotube (SWCNT) sheets. Biso and Ricci [36] reported on an IEAP actuator, which electrodes are made of multi-walled carbon nanotubes (MWCNTs). In 2006, Akle *et al*. proposed novel fabrication method called *direct assembly process* (DAP) [37] and fabricated IEAPs with high surface area RuO_2 electrodes [38]. Palmre *et al*. followed this method and proposed carbide derived carbon (CDC) [39] and carbon aerogel [40] electrodes for high-performance IEAP actuators. Torop *et al*. [41] optimized the ratios for CDC, polymer, and ionic liquid ($EMImBF_4$). Ever since in 2004 Bennett *et al*. [13] proposed ILs as stable alternatives for water solutions, IL-based actuators working in open-air environment have been emerged.

2.2. IEAP classification

Generally, IEAP materials are composed of three key components: electrode, membrane, and electrolyte (or electrolyte solution). Each can be used for classification of IEAPs. According to this principle, the list of the most popular materials for IEAP actuators is grouped by the three components in table 1.

Naturally, the boundaries between the material classes are not strict. In many works, a hybrid combination of different type of electrodes, membranes, or electrolyte solutions has shown improvement in actuator properties. For example, Plaado *et al.* [64] mixed CDC with MWCNT to improve the yield stress and strain of MWCNT electrode, Yang *et al.* [65] studied the combination of MWCNT and graphene, Nemat-Nasser and Wu [66] increased electrode conductivity by additional silver plating. Conductive metal, such as, gold has also been used for increasing the conductivity of carbon electrodes [39]. Sugino *et al.* [67] reported that using polyaniline as an additive to SWCNT electrode improves both capacity and conductivity of the IEAP.

2.3. Working principles of the IEAP actuators

In the last twenty years, numerous theories and models have been proposed to explain the electromechanical transduction of IEAP materials. In general, all authors agree that the bending of the IEAP laminates is caused by migration of the mobile ions between different layers of the laminate, and that the migration of ions, in turn, is caused by the electric field. However, the exact operating principle of each particular IEAP material is determined by its particular constituents. For example, when the membrane is made of ionic polymer, only the ions of one type – cations or anions – are mobile. In the case of non-ionic polymer membrane, both of the ions are mobile. Furthermore, the conditions of the ambient environment have direct impact on the IEAP materials, changing their operating principles. In the current work, we show that the ambient humidity has a dual effect on the behavior of the IEAP actuators, which are generally hygroscopic. It is, therefore, inevitable that the dispute about the fundamental principles among different research groups is still in progress.

Table 1. The most popular materials of IEAPs.

membrane	○ ionic polymers, ionomers ▪ Nafion® [17] ▪ Flemion® [16] ○ non-ionic polymers ▪ PVdF [36] ▪ PVdF(HFP) [42] ▪ polyethylene oxide [43] ○ polymerized ionic liquids [44]
electrode	○ metals ▪ platinum [31] ▪ gold [45,46] ▪ palladium [47,48] ▪ silver [49] ▪ copper [50–52] ○ carbons ▪ CDC [39,53] ▪ CNT [35,54] ▪ carbon aerogel [40,55] ▪ graphene [56] ○ metal oxides ▪ RuO_2 [38] ▪ ZnO [57] ○ conductive polymers ▪ polypyrrole [58,59] ▪ polyaniline [58,59] ▪ poly(3,4-ethylenedioxythiophene) [58,59]
electrolyte / electrolyte solution	○ water ○ water with electrolyte ▪ metal cations • Na^+ [60] • Li^+ [10] • K^+ [17,61] ▪ Organic cations • TMA^+ [48] • TBA^+ [60] ○ ILs ▪ cations • $EMIm^+$ [62] • $BMIm^+$ [62,63] ▪ anions • BF_4^- [62] • PF_6^- [62] • TFS^- [38,39] • $TFSI^-$ [63] ○ propylene carbonate (PC) with electrolyte ▪ LiTFSI [59] ▪ $EMImBF_4$ [59]

2.3.1. Water-based IEAPs

In 1998, Shahinpoor *et al.* published a review paper on IPMC materials. According to their work, ionic polyelectrolytes are three-dimensional network of macromolecules that are cross-linked in a nonuniform manner forming an irregular ionic charge in polymer matrix. The bending is depending on one hand on the redistribution of fixed ions and, on the other hand, on the migration of the mobile ions under electric field. According to de Gennes *et al*. [68], an IPMC actuator involves two types of transport – charge transport and solvent transport. As ions are charged and bound with water molecules, the water will be dragged along with ions causing local pressure differences near electrodes. Due to this process, one side of the material shrinks, while the opposite side expands. Naturally, if aligned in a three-layer structure, this results in a bending of a whole composite. Based on the work of de Gennes, in the same year, two other models were developed by Nemat-Nasser and Li [69], and by Tadokoro *et al*. [70]. Nemat-Nasser and Li proposed that cations under the electric field are redistributed causing a locally imbalanced net charge density. The imbalance in microscopic charge distribution acts on the polymer backbone by generating internal stresses. Under the electric field, the parts with high anion concentration shrink and the areas with high cation concentration expand. This results in the bending of the polymer membrane. Although Nemat-Nasser and Li pointed out the water transport as a possible mechanism, its contribution (in terms of polymer swelling) is considered as insignificant and the major role of actuation is suggested to be due to electrostatic forces.

Oppositely, the work by Tadokoro *et al.* [70] claims that most significantly the actuation is taking place due to the relocation of water molecules, which create local pressure gradient. The electric field causes uneven density of ions, which, being attached to the solvent molecules, form uneven solvent density. Tadokoro *et al.* also registered solvent travelling from the membrane onto the outer surface of an IPMC and the same actuating principle is in agreement with the work of Asaka and Oguro [71]. Approximately a decade later, the water transport from one electrode to another has been additionally confirmed with neutron imaging method by Park *et al*. [72].

2.3.2. IL-based IEAPs

In past decade, nonvolatile ILs have gained an increasing attention in the field of IEAPs. While replacing the water solution with an IL, the fundamentals of actuation also have to be reconsidered. Bennet *et al*. [73] reported on a study where IL-based IPMC was investigated in ambient air at various uptake of IL in Nafion® 117 membrane. This was done using Fourier transform infrared (FTIR) spectroscopy and nuclear magnetic resonance (NMR) methods. The results showed that a critical uptake of IL exists below which the actuation is negligibly small. Increasing the IL uptake above the critical point resulted in nearly proportional trend between the uptake of IL and the actuation speed.

They considered counterions of the Nafion® polymer primary charge carriers and explained the counterion transportation mechanism as hopping among sites, which are formed by loosely associated TFS^- anions.

A different *in situ* NMR study was performed by Li *et al*. [74] who conducted experiments with Nafion® NRE212 membrane swollen in EMImTFS using pulsed field gradient nuclear magnetic resonance (PFG NMR). Setting the NMR frequencies for ^1H and ^{19}F provides diffusion coefficients for both ions. The ^1H NMR can be additionally used for investigating the evaporation and reabsorption of water in IEAPs. The authors concluded that despite of the higher Van der Waals volume of $EMIm^+$ its diffusion coefficient was registered higher than that of the anion. This was confirmed regardless of the temperature and the amount of IL in the IEAP.

Imaizumi *et al*. [75] reported on actuating principles of polymer electrolyte systems, which have distinct direction of actuation. More precisely, polyurethaneurea was combined with either a lithium salt or an IL. They used ^1H, ^7Li, and ^{19}F PFG-NMR to identify the diffusion coefficients. Their physics-based model describes ion transport, which is determined by the different diffusion coefficients of cations and anions.

2.4. Back-relaxation

Throughout the development of IEAP actuators, researchers have noticed that the charge stored in the capacitive regions of the laminate is proportional with the displacement and force [38,76,77]. Nevertheless, the actuator initially responds according to the direction of ion flux, but then slowly strives back towards its neutral position, irrespective of the charged state (figure 1). The latter phenomena, which concerns universally the vast majority of the IEAP actuators, is called back-relaxation [78–80]. The same behavior is observed for blocking-force [81].

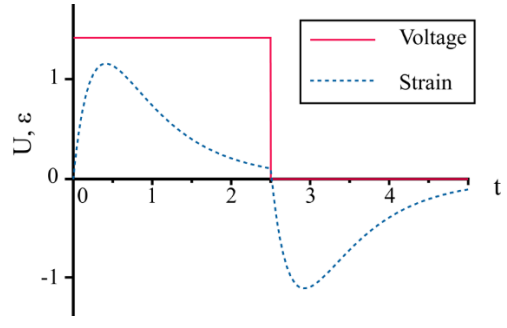

Figure 1. Principal strain response of IEAP material to step voltage input

Due to the diverse actuating principles, the dispute about the fundamental processes responsible for back-relaxation is still ongoing. In water-based IPMC actuators, the high-pressure areas near the cathode and low-pressure areas near anode are formed in the course of bending. Bao *et al.* [82] suggest that the relaxation is a result of water leakage out of the laminate, initiated by high-pressure areas towards low-pressure areas. Fujiwara *et al*. [45] explain the back-relaxation with back diffusion of water. Both theories are disapproved by the neutron imaging study, published by Park *et al*. [72]. This work shows that even after 300 seconds of stimulation with 3 V constant potential, the water gradient in IPMC persists. The authors concluded that the possible cause of relaxation is the segmental relaxation of the polymer matrix.

Many attempts try to find the correlation between the rate of back-relaxation and the constituents of the IEAP materials. Several authors have observed that the bending response of IEAP depends on the ionic radius of mobile ions [48,83,84]. More specifically, larger ions produce larger actuation, but decrease the speed of actuation related to ion diffusion rate in the IEAP. According to Nemat-Nasser [85], the ion size determines the forward actuation, but has also an influence on back-relaxation. For some cations, for example, Cs^+, the rate of back-relaxation is several times higher than the initial forward actuation. It is impossible to describe this behavior with a simple model of relocation of ions inside the IEAP. The corresponding model should incorporate other (possibly electro-chemical) processes to involve the water transport in/out of the electrodes. Kim *et al*. have demonstrated that the IPMC actuators with palladium buffer layer under the usual platinum electrode show greater bending tendency, higher blocking force, but no back-relaxation phenomenon at all. The palladium buffer layer improves the surface morphology, therefore leakage of water out of IPMC is severely limited [47].

While many publications acquiesce the back-relaxation effect, only few of them incorporate it into an electromechanical model. Yagasaki and Tamagawa [86] showed that the traditional viscoelastic models describing Maxwell and Voigt materials are not sufficient to describe all of the IPMC characteristics; hence, they modeled the relaxation of IPMC using time-dependent elastic modulus:

$$E(t) = E_0 + (E_1 t + E_2)\,\mathrm{e}^{-\lambda t}\,, \tag{1}$$

where $E_0 > E_2 > 0$ and $E_1, \lambda > 0$.

According to the work of Bao *et al.* [82], positive ions carry more water than associated in equilibrium state. Their model is described as a two-way transport. Firstly, ions with water are dragged towards cathode. Second, the surplus water diffuses back towards anode side. Bao *et al.* modeled this transport with the following differential equation:

$$\frac{dk}{dt} = K_1 \frac{dq}{dt} - \frac{1}{\tau_2}(k - K_2 q)\,, \tag{2}$$

where k is the curvature, q is the charge, K_1 and K_2 are the coefficients for bending effect that describe forward bending and the equilibrium state, respectively. τ_2 denotes the speed of back-relaxation. Fleming *et al*. [79] have demonstrated a different approach to overcome the back-relaxation effect. By patterning the IPMC actuator into several electrically independent electrodes they have mitigated back-relaxation of the whole device through feedforward and feedback control of the electrically separate, but mechanically joined segments of the device.

2.5. Effects of operating environment

2.5.1. Humidity

Charged particles in IEAPs associate well with polar molecules, such as water. While this is just a common knowledge related to the actuating principles of water-based IEAPs, it is often missed when operating IEAPs in ambient air that contains humidity. NMR studies on IL-based IEAPs confirm that, although not primarily responsible for actuation, the water has a significant influence on viscosity, ionic conductivity, diffusion coefficient, etc. [73,74]. The fluctuation in these parameters contributes directly to the overall electrical and mechanical performance noticed by many authors. Hao *et al*. [87] showed that the blocking force of a water-based IEAP actuator is highly reliable on its water content, which, if operating the IPMC in an open air environment, decreases (evaporates) over time. Kikuchi *et al*. [88] used FTIR to determine the absorbed water content of IL-based IEAPs. Although the humidity affected the rate of actuation, the charge to curvature ratio was found close to linear for all measurements, regardless of the ambient relative humidity (RH) level. Must *et al*. [89] reported that humidity in IEAPs does not necessarily have to be avoided. As the water increases ionic conductivity and shifts the diffusion limit towards higher frequencies, an order of magnitude higher displacement was observed at 5 Hz harmonic signals. On the contrary, a considerable effect of back-relaxation was also registered at frequencies below 0.5 Hz for RH above 74%.

2.5.2. Temperature

The flow of charge to the electrical double-layer of the IEAP laminate is limited by multiple electronically resistive parts. These parts are addressed to ohmic drop and release heat proportionally to the square of the electric current. Several studies report on the effects of ambient temperature on various IEAP constituents. However, there exist only few papers, which consider Joule heating in the IEAP when it is actuated. The first thermal heating effects of water-based IPMCs were reported by Shahinpoor and Kim [10] in 2001. They observed a temperature rise of more than 10 °C after applying a DC voltage of 3 V. Akle and Leo [84] monitored the temperature of an IL-based IEAP by an attached

thermocouple. After 400 seconds of 2 V sine wave excitation the temperature increase of 0.35 °C was reported. In a recent study, Punning *et al*. [11] compared the heating of various IEAPs using infrared thermal imaging and low frequency pulses between ±3.5 V. They reported surface temperatures reaching from room temperature to over 85 °C in about 30 seconds.

From the perspective of an efficient IEAP actuator, Joule heating is an unwanted waste of energy. Nevertheless, Kruusamäe *et al*. [90] considered it as an advantage and used it for shape-fixing of IEAPs. The technique relies on high frequency driving signal, which causes an elevated temperature and figuratively melts the polymer for short time.

Since the thesis at hand is focused on investigating step input responses of IEAP actuators, the current peaks instantly and then decays in time as the actuator charges up. The highest thermal effects take place in the very first moments after the step input is applied. Since the experimental part of this dissertation involves IEAP samples with relatively high internal resistance, the current consumption throughout the experiments is limited to below a few mA. This allows the thermal effects to be considered as out of scope.

3. SCOPE OF RESEARCH

The term “IEAP” roughly embraces all electrically active ionic materials, which contain polymer and respond to electrical stimulus. The scope of the thesis at hand includes only the IEAPs, which operate because of ion migration and charging of electrical double-layer, that is, no faradaic redox processes are considered as primary working mechanisms. Therefore, from this point forward, the meaning of IEAP is strictly confined to electromechanical materials where the conversion from electrical domain to mechanical domain is obtained by direct electromechanical conversion.

The thesis at hand is focused on IEAP materials in actuator configuration, with the main aim on modeling and characterizing the electromechanical effects, especially the back-relaxation that takes place under the step input voltage. The IEAPs are analyzed in freely bending mode. If not stated otherwise, the geometry of the tested IEAP samples is a rectangle. The samples are chosen from the IEAP materials that are capable of operating in gaseous environment, and they are tested in different ambient conditions including vacuum, humid air and dry air.

This work focuses on gray-box modeling approach, which has a good balance between all-inclusive white-box description and black-box abstraction. In gray-box modeling, the IEAP actuators are represented with electrical and mechanical equivalent circuits. The macro-scale parameters (dimensions, the modulus of elasticity, resistance of electrode, double-layer capacitance, etc.) are preserved, allowing scalability of the model from one actuator to another.

This thesis contributes with an electromechanical model where the back-relaxation effect is interpreted using viscoelastic elements. First, the models are verified for various IEAP types. Next, the model is used for characterizing IEAP materials in varying ambient conditions. Finally, two IEAP materials, which differ only in terms of the membrane material, are characterized and compared in varying ambient conditions. The results show clear correlation between the rate of back-relaxation and the level of relative humidity of the surrounding environment.

The objective of this dissertation is:

- to develop a generalized distributed model that is able to address back-relaxation and take into account electrode resistance;
- to provide necessary tools/methods for characterizing IEAPs in variable environmental conditions;
- to apply the developed method to characterize the effect of humidity on the performance of nanoporous carbon based IEAP under DC step voltage input stimulus:
    - forward actuation,
    - back-relaxation.

4. MODELING

4.1. Introduction

Modeling is essential in understanding and describing the electromechanical and mechanoelectrical behavior of IEAP materials. It allows one to estimate how various parameters (for example dimensions, conductivities, mechanical rigidity) change the characteristics of the IEAP device and serves as an important starting point for developing accurate controllers. As the design and manufacturing of the IEAPs have always been tightly entangled with modeling and optimization, the first models of IEAPs were made available already since 1998 by Firoozbakhsh, Shahinpoor, and Shavandi [91]. They modeled coulombic attraction/repulsion between metal electrode particles and sulfonic groups attached to the polymer network. According to their work, an optimal structure for force and motion should consist of series of miniaturized muscle strips similar to that of myofibrils in biological muscles. Since that time, different approaches and modeling strategies have been introduced, which roughly classify the models into white-, gray-, or black-box category.

Black-box model is an abstract system, which concerns only an input and output. The body of the system is presented with mathematical relations (for example a polynomial function) that rely on a certain number of parameters. The parameter values are obtained from process called system identification, which matches the relations between input and output using various fitting techniques. Next, the identified parameters are verified using some input signal, different from the one that was used for identification. Since black-box model parameters are typically not interpreted as physical quantities, the scalability from one actuator to another is limited. Thus, for each system a separate identification is required.

The models, which describe IEAP materials with low-level physical, electromechanical, and electrochemical processes, are known as white-box models. For example, electro-osmosis [71,92], ion transport [70,93,94], or changes of stress, strain, temperature, humidity are of interest. It might take a lot of effort to identify the parameters of a white-box model experimentally. Even if the parameters of each constituent of an IEAP can be separately determined, due to the interaction between constituents and the impact of the manufacturing process, these properties in the assembled composite will very likely be different.

White-box models are worthwhile to clarify the complicated fundamentals of an IEAP actuator, but result in large number of relations and parameters that overcomplicate the solving procedure. Hence, the majority of white-box models are solved using numerical methods. A comprehensive example of using finite element method (FEM) for describing the electromechanical processes of an IPMC actuator is presented by Pugal *et al.* They developed a model according to the Nernst-Planck-Poisson-Euler equations [93] and improved computational solving time by adaptive multi-meshing and adaptive refinement of the polynomial degree [95,96].

From the engineering perspective, a preferred model is a trade-off between white- and black-box models – so called gray-box model. Gray-box models use the knowledge about the complicated underlying processes and present the system with simplified equivalent elements such as resistors, capacitors, Warburg elements, constant phase elements, springs, dampers, etc. The named electrical and mechanical elements are connected into a network to develop simple yet scalable models. Usually the gray-box model parameters (for example dimensions, elastic modulus, resistance of electrodes, etc.) can be identified from simply conducted measurements.

In this section, a quantitative model for straightforward characterization of IEAP actuators is presented. The essence of distributed representation and modeling of IEAP devices is clarified. Then, an electromechanical model incorporating the standard elements of viscoelasticity – spring and damper – is proposed for describing the forward bending accompanied with back-relaxation. Finally, a distributed electromechanical model with relaxation will be introduced.

4.2. IEAP representation and characterization

4.2.1. Geometry and boundary conditions

IEAP actuators are highly customizable devices, which manufacturing routines and geometry may vary depending on the target application. As an example, a non-traditional rod-shaped IEAP actuator with patterned outer electrodes has been demonstrated by Palmre *et al*. [97]. However, as a rule, characterization of IEAP samples is carried out with rectangular samples. In order to prevent curling and bending in the width direction the aspect ratio of width to length is typically less than 1:3. The IEAP of that shape can be described as a cantilever beam with one end electrically and mechanically fixed between rigid contacts. The other end either is free to bend, or simply supported while being blocked by a force gauge.

4.2.2. Performance evaluation

To date, the most adopted method for characterizing the performance of IEAP actuators is determining their transverse displacement with a distance sensor (for example laser sensor). Since the result is registered at a specific point on an IEAP, comparing the results amongst actuators of different dimensions and types requires the measured quantities to be normalized. Therefore, the acquired transverse displacement is recalculated with respect to distance from contacts, material dimensions, elasticity, etc.

Assuming that the actuator bends to a perfect circle [6] (see figure 2), the measured transverse displacement δ at distance L from fixed contacts can be expressed as curvature κ or radius of curvature R as [98,99]

$$\kappa = \frac{1}{R} = \frac{2\delta}{L^2 + \delta^2}. \tag{3}$$

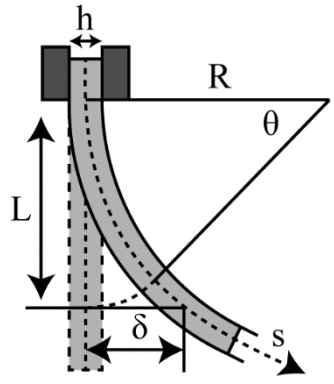

Figure 2. Displacement measurement geometry

The exact difference of strain between the opposite electrode layers ε_d is given in [67] as

$$\varepsilon_d = \frac{\Delta L_1 - \Delta L_2}{L} = \frac{h}{R}\left(1 + \frac{\Delta L_1 + \Delta L_2}{2L}\right), \tag{4}$$

where h is the thickness of the whole IEAP, $L + \Delta L_1$ and $L + \Delta L_2$ are the lengths of electrode layers during bending. Usually, the rightmost term of equation (4) can be considered negligibly small and the equation simplifies to [10,67]

$$\varepsilon_d \cong \frac{2h\delta}{L^2 + \delta^2}.$$

It is important to distinguish the strain difference ε_d and bending (or normal) strain ε. While ε_d specifies difference of strains between the two electrode layers, the actual expansion/contraction in the IEAP, described with the bending strain ε, remains unknown. In fact, the number of combinations of bending strains that can produce the same strain difference and curvature is infinite.

When, the IEAP shows symmetrical behavior, its actual bending strain can be uniquely found according to traditional analysis of cantilever beams. Since the bending strain is proportional to the distance from the neutral plane, the maximum bending strain ε at outer electrode layers becomes

$$\varepsilon = \frac{h}{2}R. \tag{5}$$

The bending strain is equal to the half of the strain difference only when bending is symmetrical with respect to the centroid of the beam:

$$\varepsilon = \frac{1}{2}\varepsilon_d. \tag{6}$$

The classical theory of cantilevered beams assumes that the strains are symmetrical and the neutral layer positions exactly to the centroid of the beam. The same analogy is often assumed for IEAP actuators. Nevertheless, we have analyzed the internal strains of various IEAP materials and concluded that not all IEAPs follow this assumption. In other words, depending on the IEAP type the actuator might expand or contract asymmetrically along the laminate plane altering its width, length, and thickness without contributing to bending. Thus, a proper verification is essential before continuing with equation (6).

Neither the strain difference nor the curvature directly give information about the actual forces and internally generated moments in the IEAP. For example, an IEAP with rigid structure and high effective bending stiffness is capable of generating high blocking forces, but its bending amplitude and speed are rather limited. A good parameter for characterization of the blocking force as well as the bending ability of an IEAP actuator would be the electrically induced bending moment. Knowing the bending stiffness of the IEAP, electrically induced bending moment is expressed as

$$M_E = EI\kappa\,, \tag{7}$$

where κ is the curvature of the actuator, E is the effective Young's modulus of the IEAP material and I is the second moment of area of the beam. As the IEAP cross-section is a rectangle, I becomes

$$I = \frac{bh^3}{12} + bh\Delta^2, \tag{8}$$

where Δ denotes the distance from the neutral layer to the centroid of the beam. It is often assumed that the neutral axis of the beam coincides with the centroid of the IEAP laminate (that is beam is bending symmetrically). Since the deviation of the neutral axis from the centroid Δ in equation (8) is squared, the additional term introduces a huge correction to the area moment of inertia. For example, when the neutral layer is located at the boundary of the membrane ($\boldsymbol{\Delta}= h/2$), I increases as much as four times:

$$I = \frac{bh^3}{12} + bh\left(\frac{h}{2}\right)^2 = 4\left(\frac{bh^3}{12}\right) \tag{9}$$

Another quantity that takes into account the bending stiffness EI, is the strain energy U. Strain energy expresses the mechanical work that is required for bending the beam to a curvature of $1/R$. This parameter is commonly used for estimating the efficiency factor of the IEAP actuators. It is defined with the relation

$$U = \frac{EIL}{2R^2}\,. \tag{10}$$

The equations (7) and (10) show that these particular two parameters – induced bending moment and strain energy – involve the evaluation of two mechanical characteristics: bending displacement and blocking force.

4.2.3. Distributed representation of IEAPs

It is convenient to estimate the behavior of the whole IEAP actuator from observations taken at a single point of the actuator. A generally accepted practice is evaluating the tip displacement or blocking force measured at a predefined distance from the clamp of the beam. Naturally, that kind of generalization involves several prerequisites and assumptions that have to be carefully considered:

- electromechanical properties (for example, Young's modulus and charge-to-strain ratio) and the dimensions of the cross-section of an actuator are invariable along its length;
- the thicknesses of both electrodes are equal and invariable in time;
- the curvature along the actuator is uniform and the bent IEAP forms an exact arc of a circle;
- strain formulas are valid for small displacements only;
- neutral layer of bending positions at the centroid of the IEAP cantilever;
- displacement between the fixed contacts and measurement point is considered insignificant during blocking force measurements.

Depending on the electrical and mechanical parameters of a particular IEAP, many of the abovementioned assumptions might easily fail. For example, when the lengthwise conductivity of the electrodes is an order of magnitude lower than the conductivity along the thickness direction of the laminate, the actuator charges unevenly, producing uneven bending in time. Alternatively, similar result can be obtained when the laminate charges uniformly, but its bending stiffness varies, for example, due to thermal effects. To study and model possible fluctuations along the length of IEAPs, we need a distributed representation of the IEAP beams. Instead of a single value of curvature, strain, blocking force, or bending moment, the one-dimensional distributed representation evaluates those quantities as a function of the distance from the fixed input contacts, along the curve.

A variety of approaches of describing the uneven bending of the IEAP beams has been reported. Kim and Kim attached special markers to an IEAP actuator and tracked their position with a camera [78]. A distributed force map of an IEAP actuator has been provided by Martinez and Lumia [94]. A sequence of scanning electron microscope images combined with digital image correlation technique [99] additionally enables a close up analysis of strains in the IEAP.

In this thesis, we record the IEAP from its side with a video camera. The proper back-illumination allows obtaining contrast projections of the IEAP shape, as demonstrated in figure 3.

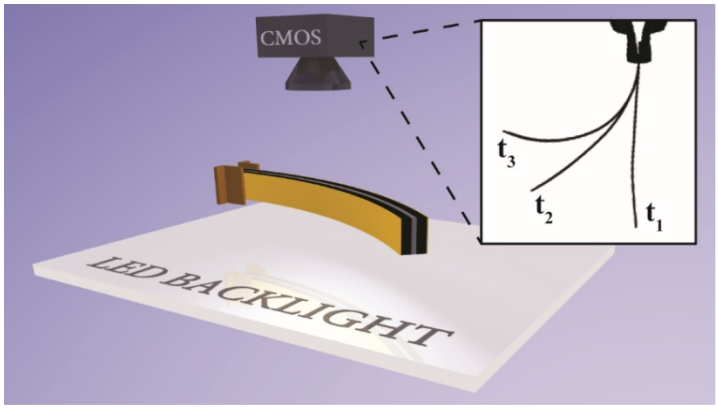

Figure 3. Acquisition setup of distributed bending

As our aim is to extract the local curvature $\kappa(s)$ for $\{s \mid 0 \le s \le L\}$. Taking into account that the local curvature is a derivative of the local angle $\varphi(s)$

$$\kappa(s) = \frac{d}{ds}\varphi(s), \tag{11}$$

we track the pixel line and divide it into finite number of vectors with equal lengths, as shown in figure 4. A constant curvature along each vector is assumed and the change of orientations of adjacent vectors is then proportional to the local curvature. As a result, the total time-dependent distributed mechanical behavior of the actuator can be presented with a 3-dimensional matrix or graph (see figure 5).

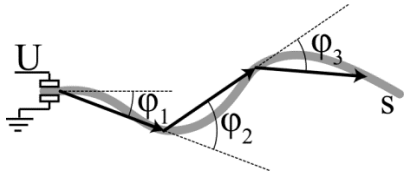

Figure 4. Vector representation

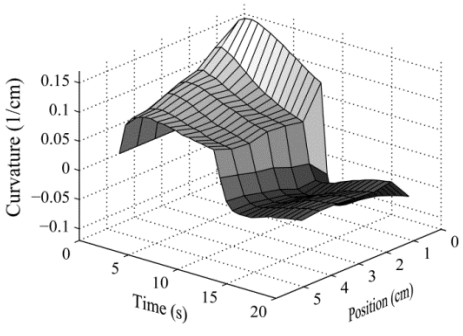

Figure 5. Transient behavior of an IEAP actuator

The method is universal and serves as a key step in characterizing and modeling the distributed bending of the actuators. The initial undeformed shape of IEAP may be arbitrary, which can be subtracted when tracking the changes in curvature. The described vector representation is beneficial for examining the distributed mechanical response of IEAP, verify the feasibility of circular approximation, and analyze the homogeneity of the laminate.

4.3. Electromechanical modeling

Over all, the gray-box electromechanical models of IEAP actuators consist of an electrical part Z and a mechanical part M, linked by an electromechanical coupling $\varkappa$ as depicted in figure 6.

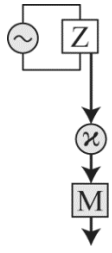

Figure 6. Generalized electromechanical gray-box model of IEAP

The input of the model is an electrical excitation (voltage or current), and the output is a mechanical response (displacement, strain difference, curvature, etc.). The coupling $\varkappa$ describes a relation between the electrical and mechanical part and it is commonly obtained by an intuitive analysis of experimenting with the real IEAP samples.

4.3.1. Electrical equivalent circuits

Simplistically, IEAPs have capacitive characteristics. When the voltage is applied to the electrodes, the potential between electrodes gradually increases. Therefore, a rough electrical equivalent circuit of IEAP consists of capacitors representing a double layer interfaces in both electrodes and resistors representing the bulk resistance of electrodes as well as the resistance of ionic media (see figure 7A). According to the rules of electrical circuits, the series of connected capacitors and resistors can be grouped to a canonical form of single R–C chain shown in figure 7B.

An ideal IEAP has its electrodes completely separated without electronic conductivity between them. However, due to the manufacturing imperfections, the real IEAP samples may have micro shortages, which cause excessive current that dissipates in the form of Joule heating. We reflect that with additional resistor, added in parallel with the R–C chain as shown in figure 7C–E. Notice that the equivalent schemes depicted in figure 7C–E can be simplified to canonical forms shown in figure 7F and figure 7G.

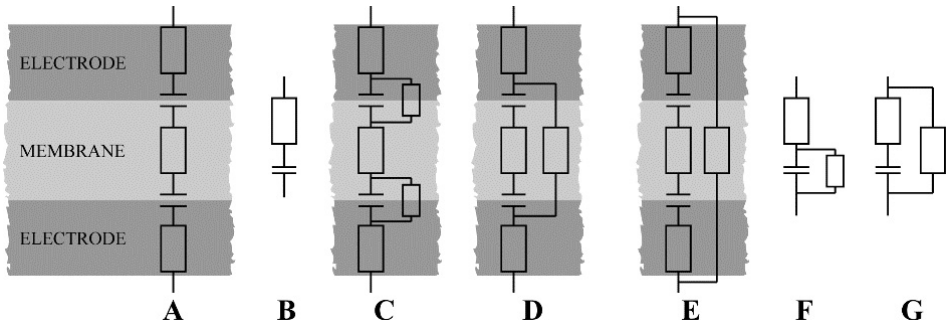

Figure 7. Electrical equivalent circuits

The presented R–C chain is relatively accurate approximation to describe the charging of IEAPs with thin electrode layers. However, in order to optimize the actuator for maximum force output, highly capacitive and relatively thick electrodes are needed. Experimenting with 170 µm CDC electrodes has revealed that the match between the simulated and experimentally measured current is rather coarse and not sufficient to adequately describe the total charging/discharging curve. Since the conductivity of CDC electrodes is relatively low (reported in the order of 5×10^{-4} S/cm [39,41]), during charging, the potential drop along the electrode thickness becomes significant. The gradual charging in the thickness direction has been deliberated earlier by Bao *et al*. [82], who proposed distributed R–C transmission line model for explaining the fractal structure of platinum dendrites in IPMC. The experimental measurements in this thesis bring out that for carbon-based actuators with thick electrodes, two parallel R–C chains (shown in figure 8) is sufficient for describing the electrical behavior. The two R–C chains can be interpreted as double-layer charging with two different time constants. This means that the actuator is virtually divided into two regions. The first region charges quickly and involves ions that can easily access to the double layer interface. In the second virtual region, the charging is restricted by the electronic resistance of electrodes and by the migration of ions towards the deep and hardly accessible pores. The electrical model incorporates also a resistor R_{SS} that models the steady-state current.

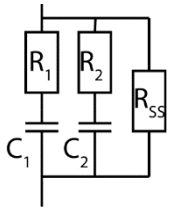

Figure 8. Electrical equivalent for thick CDC electrodes

It is important to note that the models proposed in this thesis are designed and verified for step responses of IEAP actuators. Nevertheless, when harmonic signals are of interest, additional elements, such as a Warburg element in parallel with the capacitors [77,100] has improved the impedance match.

4.3.2. Mechanical interpretation of back-relaxation

The mechanical response (that is stress-strain relationship) of linear elastic materials (for example, steel) can be described with Hooke's law

$$\sigma_S = E\varepsilon \tag{12}$$

where the mechanical stress σ_S and strain ε are proportionally coupled via Young's modulus E. On the contrary, the mechanical response of liquids involves viscous friction that is modeled with a dashpot relating mechanical stress σ_D with strain rate $d\varepsilon / dt$ by viscosity η as

$$\sigma_D = \eta \frac{d\varepsilon}{dt}. \tag{13}$$

In general, the mechanical response of polymer materials unveils both elastic and viscous properties [101], which are modeled using viscoelastic models [102] such as Kelvin-Voigt, Maxwell, and standard linear solid models, depicted side by side with the corresponding equations in figure 9.

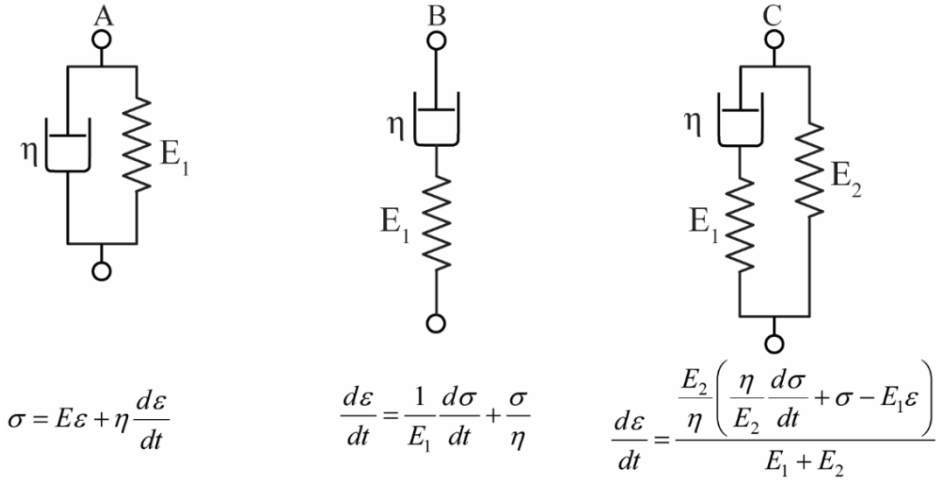

Figure 9. Three viscoelastic models: A – Kelvin–Voigt; B – Maxwell; C – standard linear solid model

These models are composed of primitives such as springs and dampers. Spring elements describe the energy storage, while the dashpots represent dissipative losses in viscous media. Furthermore, the behavior of dashpots is similar to relaxation of polymer chains and enables modeling phenomena such as creep or stress relaxation. The classical viscoelastic models are designed for external excitation. As the excitation in IEAP materials is internal, these cannot directly be tailored for IEAPs and different mechanical interpretation is required.

In this dissertation, a new mechanical scheme for modeling the back-relaxation of IEAP actuators is given. Inspired from Kelvin-Voigt model (see figure 9A), a dashpot is aligned in parallel with a spring. An internal strain element **Q** (associated with the transient electrical charge q of the IEAP material) is added in series with the dashpot. The element **Q** serves as an input of the mechanical model and it is coupled with the accumulated charge in electrical double layer interface. To indicate its magnitude, we portray the internal strain element **Q** between arrows as depicted in figure 10.

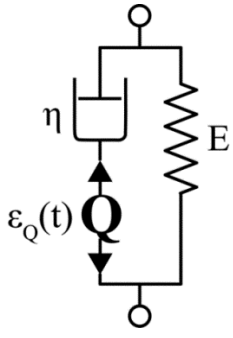

Figure 10. Mechanical model of back-relaxation

When the internal strain ε_Q of the element **Q** is introduced, the spring responds instantly, expanding–contracting the elastic threads of the polymer molecules network. The damper follows with time, tending towards the unstressed state of the spring. Physically speaking, the dashpot resembles the flow resistance (viscosity) of liquid phase (electrolyte solution or ionic liquid) that migrates from high-pressure area to low-pressure area. The speed of how fast the model reaches its relaxed state is determined by the ratio of E and η, known from Kelvin-Voigt model as the rate of relaxation $\lambda = E / \eta$. In brief, the input of our mechanical system is the strain ε_Q, while the output is the strain of the spring ε_S.

Figure 11 demonstrates the response of the mechanical model at different time instances. Initially (figure 11A), all elements are in their unstressed state. Any change in element Q will expand or contract the spring (figure 11B and figure 11D), while the dashpot slowly dissipates stress from the spring allowing the spring to relax towards its unstressed state (figure 11C and figure 11E).

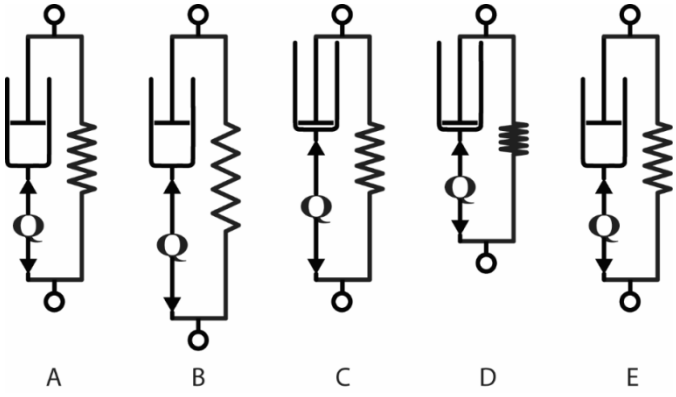

Figure 11. Working principle of the mechanical model

By considering relations (12)–(13) and taking into account the element layout, the mathematical representation of the model becomes

$$\varepsilon_S(t) = \varepsilon_Q(t) - \lambda e^{-\lambda t} \int_0^t \varepsilon_Q(\tau)\, e^{\lambda \tau} d\tau, \tag{14}$$

where ε_Q is the strain generated according to the electrical model, ε_S is strain of the spring element that serves as output, and λ denotes the speed of relaxation.

4.3.3. Electromechanical coupling

Several authors [76,88,103] have approved that a proportional coupling between electrical charge stored in the double-layer and mechanical domain (that is, stress or strain difference, bending moment, curvature, transverse displacement, etc.) is a good approximation to start with. This dissertation follows the same concept by supposing that the electrically induced bending moment M_E is proportionally related to charge q as

$$M_E = \mu q\,. \tag{15}$$

Since we consider the IEAPs as a cantilevered beam in which only electrically induced bending moments are taken into account, from (7), we can couple charge directly to curvature

$$\kappa = \alpha q\,, \tag{16}$$

where $\alpha = \mu / EI$. Nevertheless, the proportional coupling is not sufficient for adequately modeling long-term (low frequency) bending of IEAPs. When the IEAP is excited with a step input signal, it first bends proportionally to the

inserted charge. Due to internal stresses, the material slowly relaxes towards its initial position, without any changes in electrical charge. In order to describe this phenomenon adequately, a more sophisticated coupling or mechanical model is required.

Next, a mechanical model that is able to handle relaxation of IEAP materials was developed.

Recalling chapter 4.3.1, we found that the electrical model which consists of single R–C chain, gives adequate fit ($R^2 > 0.99$) only for some specific type of IEAPs. For other types, the fit is poor ($R^2 < 0.6$). It was observed that the mismatch comes from thick electrodes, which require considering the transmission line effect in thickness direction. Chapter 5 approves that approximating the electrical transmission line in the thickness direction to two R–C chains is sufficient to obtain good fit ($R^2 > 0.9$) for several environments and potentials. Here we develop the electromechanical models for both thin (figure 12A) and thick (figure 12B) electrodes.

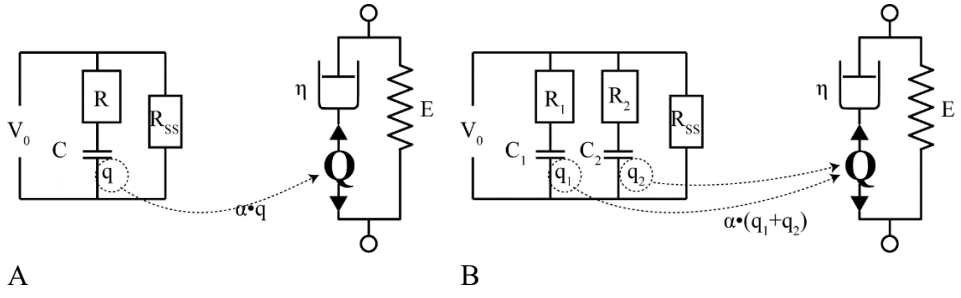

Figure 12. Electromechanical model for IEAPs with (A) thin and (B) thick electrodes

When the actuator is initially discharged $q(0) = 0$ and the circuit is connected to DC input with voltage of V_0, the charge $q_C(\mathrm{t})$ accumulating in capacitor is expressed as

$$q_C(t) = CV_0(1 - \mathrm{e}^{-\frac{t}{RC}}). \tag{17}$$

Bringing together the electrical model (17) and the mechanical model (14), we obtain an electromechanical formulation for time-dependent curvature

$$\kappa(t) = \frac{\alpha CV_0\left(\mathrm{e}^{-\frac{t}{\tau}} - \mathrm{e}^{-\lambda t}\right)}{\tau\lambda - 1}, \tag{18}$$

where $\tau = RC$ and α is the proportional electromechanical coupling coefficient between electrically induced charge and curvature, and λ is the rate of

relaxation. For thick electrodes, we use the electrical equivalent circuit proposed in section 4.3.1, in which the total charge is given as

$$q(t) = V_0 \left[C_1 \left(1 - \mathrm{e}^{\frac{-t}{\tau_1}} \right) + C_2 \left(1 - \mathrm{e}^{\frac{-t}{\tau_2}} \right) \right], \tag{19}$$

where $\tau_1 = R_1 C_1$ and $\tau_2 = R_2 C_2$. The corresponding electromechanical coupling can then be expressed as

$$\kappa(t) = \frac{\alpha V_0 \left[C_1 (\tau_2 \lambda - 1) \mathrm{e}^{\frac{-t}{\tau_1}} + C_2 (\tau_1 \lambda - 1) \mathrm{e}^{\frac{-t}{\tau_2}} - \left(C_1 (\tau_2 \lambda - 1) + C_2 (\tau_1 \lambda - 1) \right) \mathrm{e}^{-\lambda t} \right]}{(\tau_1 \lambda - 1)(\tau_2 \lambda - 1)}. \tag{20}$$

The obtained function has two poles, which does not allow determining, which of the two time constants of charging becomes equal to the time constant of relaxation. Theoretically, in that case, all of the generated bending will be instantly canceled out by relaxation. However, in real IEAP systems, the time constant of charging time is orders of magnitude higher than the time constant of relaxation leaving the poles off the subject. To exemplify the capabilities of the two electromechanical models, equations (18) and (20) are simulated with a set of arbitrarily selected parameters in figure 13A and figure 13B.

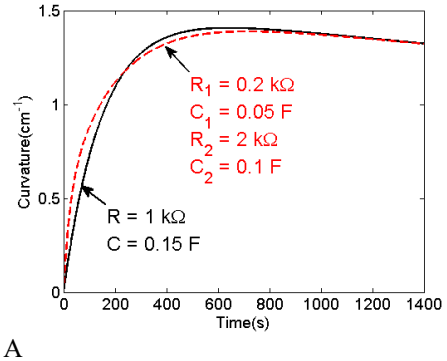

A

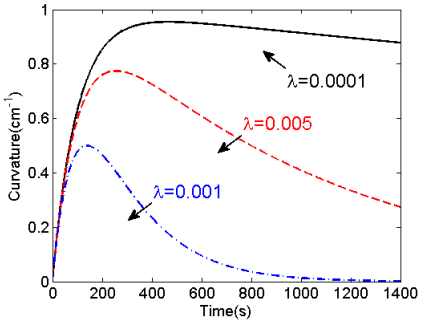

B

Figure 13. Simulated curvatures with parameters $\alpha = 10\ \mathrm{C^{-1}cm^{-1}}$ and $V_0 = 1\ \mathrm{V}$; A – comparison of models with one and two R–C circuits with fixed $\lambda = 1 \times 10^{-4}\ \mathrm{s}$; B – comparison of various relaxation rates with fixed $R_1 = 0.2\ \mathrm{k\Omega}$, $C_1 = 0.05\ \mathrm{F}$, $R_2 = 1\ \mathrm{k\Omega}$, and $C_2 = 0.1\ \mathrm{F}$

4.4. Distributed modeling

4.4.1. Introduction

So far in this chapter, the behavior of IEAPs has been modeled with a single electromechanical equivalent circuit, which considers the resistance of electrodes in their thickness direction only, suppressing the fluctuations along the longitudinal axis. However, for several types of IEAPs, the lengthwise electrode conductivity is comparable with that of across the electrode. Then it can no longer be assumed as not significant and the distributed modeling approach becomes inevitable. In a distributed gray-box model, an additional dimension is added for representing the lengthwise effects with multiple cross-sectional lumped equivalent circuits (introduced in 4.3.1). The lumped units are joined together through elements that resemble the impedance of the electrodes along their length, depicted in figure 14.

The state-of-the-art fabrication of IEAPs used in this work involves the porous carbon-based electrodes with an additional layer of highly conductive current collector – a gold foil. The purpose of this enhancement is to improve the actuation performance by increasing the lengthwise conductivity of electrodes by several orders of magnitude. In principle, for those IEAPs, the distributed modeling approach is not relevant. However, since the gold layer is brittle and vulnerable to scratches caused by externally touching objects, it could easily lose its conductivity, instantly requiring a distributed modeling approach.

In this subsection, we develop a distributed model that is able to involve the effects of electrode resistance along the material. The distributed electrical model is then coupled with mechanical model of relaxation (see chapter 4.3.2), which results in a distributed gray-box model capable of describing the forward bending as well as back-relaxation of IEAP actuators.

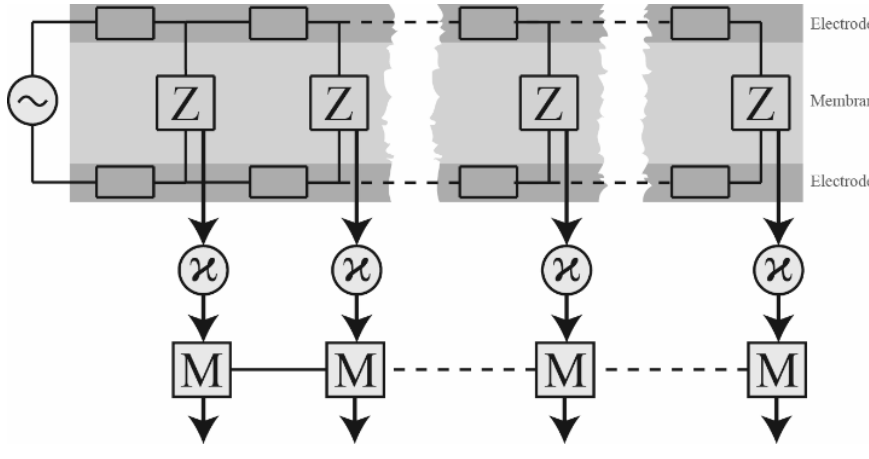

Figure 14. A generalized distributed electromechanical model of IEAP actuator

4.4.2. Electrical model

This thesis focuses on carbon-based materials, which lengthwise measured electrode impedance is taken as simple resistor. This assumption is made in accordance to the previous study by Kruusamäe *et al*. [104], which concludes that there is no significant capacitive component along the CDC electrodes. We demonstrate the distributed approach using the lumped equivalent circuit that was given in figure 7G. Its distributed form, depicted in figure 15, is identical to what is used for long electrical transmission lines, described with Telegrapher's equations by Oliver Heaviside [105]. The same concept was adapted and verified for IPMC actuators by Punning *et al*. [103]. In this thesis, we further broaden the range IEAP types that this distributed equivalent circuit can handle.

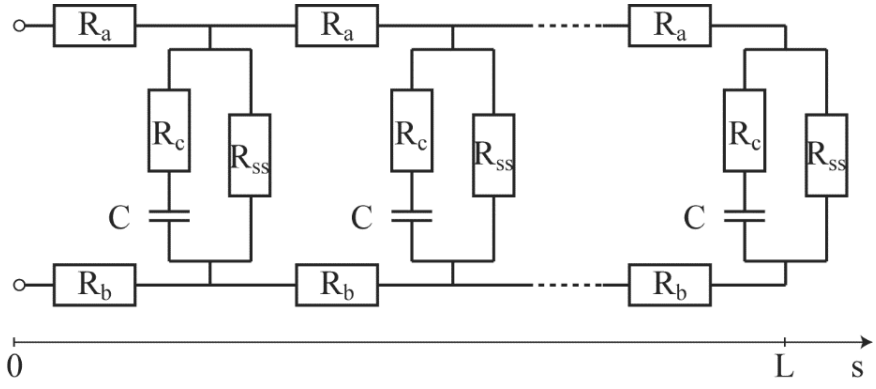

Figure 15. Distributed electrical equivalent circuit of IEAP actuator

Mathematically, the essence of distributed model is given with respect to Ohm's law and Kirchhoff's principle of charge conservation

$$\frac{\partial v(s,t)}{\partial s} = -R_e \cdot i(s,t), \tag{21}$$

which says that any change in potential along the length of the IEAP actuator is proportional with the transverse current between electrodes at that point, and $R_e = R_a + R_b$. The general partial differential equation for propagation of coordinate- and time-dependent voltage $v(\mathrm{s},t)$ between the two electrodes is expressed as

$$\frac{\partial^3}{\partial x^2 \partial t} v(x,t) + \frac{1}{R_c C} \frac{\partial^2}{\partial s^2} v(s,t) - R_e \left(\frac{1}{R_c} + \frac{1}{R_{ss}} \right) \frac{\partial}{\partial t} v(s,t) - \frac{R_e}{R_c C R_{ss}} v(s,t) = 0. \tag{22}$$

When the IEAP is initially discharged $q_C(s,0)=v(s,0)=0$, its one end is subjected to an input step voltage $v(0,t)=V_0$, and another end is left open $(\partial/\partial s)v(L,t)=0$, the analytical solution for equation (22) is given in [106] as

$$v(s,t)=V_0\left[\sum_{n=1}^{\infty}\left(-b_n\sin\left(\frac{2n-1}{2L}\pi s\right)e^{-k_n t}\right)+\frac{\cosh\left(\sqrt{\frac{R_e}{R_{SS}}}(s-L)\right)}{\cosh\left(\sqrt{\frac{R_e}{R_{SS}}}L\right)}\right], \tag{23}$$

$$\text{where } k_n=\frac{W\left(\frac{4R_e}{R_{ss}}L^2+\pi^2(2n-1)^2\right)}{C\left(\pi^2(2n-1)^2+4R_eL^2\left(\frac{1}{R_{ss}}+\frac{1}{R_c}\right)\right)} \text{ and } b_n=\frac{4\pi(2n-1)}{\pi^2(2n-1)^2+\frac{4R_e}{R_{ss}}L^2}. \tag{24}$$

Then, the charge on the capacitor can be obtained from the transient voltage as

$$q(s,t)=\left(\int_0^t\frac{1}{R_c}v(s,\tau)\mathrm{e}^{\frac{1}{R_cC}\tau}d\tau\right)\mathrm{e}^{-\frac{1}{R_cC}t}. \tag{25}$$

As can be seen from (23), the transient voltage is given with infinite series. However, the series converges fast and is suitable for numerical evaluation. The impact of the number of terms on the voltage distribution with arbitrarily chosen parameters $V_0=1.5$ V, $R_e=50\ \Omega\ \mathrm{cm}^{-1}$, $C=0.1$ F cm^{-1}, $R_C=100\ \Omega\ \mathrm{cm}^{-1}$, $R_{SS}=10$ k$\Omega\ \mathrm{cm}^{-1}$, $N=200$ is depicted in figure 16.

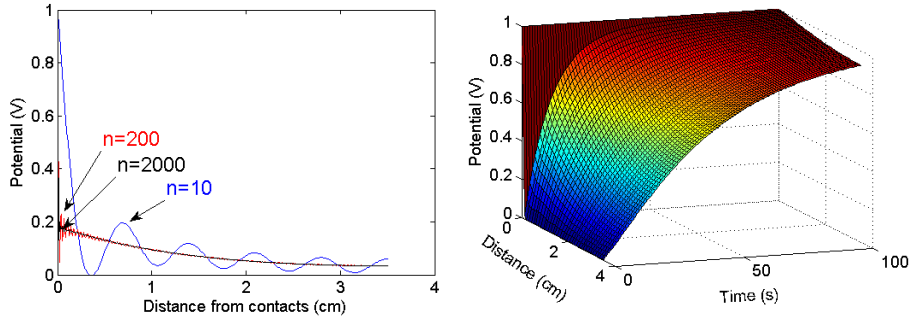

Figure 16. Simulated transient voltages; A – the convergence at t=2 s with different number of terms; B – transient voltage in time with N=200

4.4.3. Electromechanical model

In the present distributed modeling approach, the charge is depending on the coordinate along the length of IEAP. This means, that the charge at each particular position on the beam generates a corresponding bending moment and curvature, which have to be deliberated as coordinate-dependent functions as well. Although mathematically continuous, in practice, the distributed shape of an IEAP can be represented with a finite number of vectors as was introduced in section 4.2.3. One can think of the model as a discretized multilink manipulator depicted in figure 17.

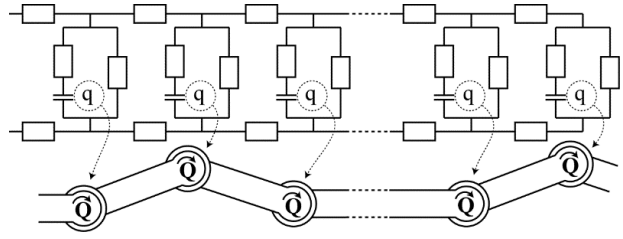

Figure 17. Distributed electromechanical model of IEAP

Currently, we are not concerned about any changes in mechanical parameters along the length of the beam, meaning that elastic modulus, second moment of area, charge to bending moment coefficient, and the relaxation rate are considered invariable. That said, identically to the one given in section 4.3.3, the local charge is related to the local curvature as

$$\kappa(s,t) = \mu\left[q(\mathrm{s},t) - \lambda e^{-\lambda t}\int_0^t q(\mathrm{s},\tau)\, e^{\lambda\tau} d\tau \right]. \tag{26}$$

The simulation results with V_0=1.5 V, R_e=200 Ω cm^{-1}, C=0.2 F cm^{-1}, R_C=100 Ω, R_{SS}=10 kΩ, α=10 with two different values of λ are shown in figure 18.

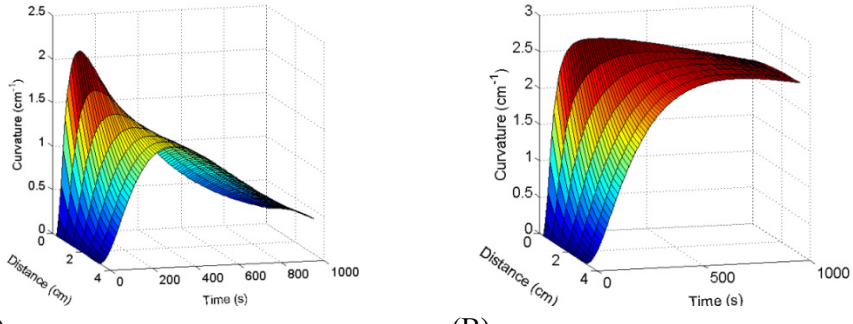

(A) (B)

Figure 18. Simulated curvature along the IEAP actuator in time; (A) – λ=2×10^{-3}; (B) – λ=3×10^{-4}

5. EXPERIMENTAL

5.1. IEAP materials

The thesis at hand involves three different kind of IEAP materials that are used for distributed model verification, long-term characterization, and investigating the influence of the ambient operating environment. Hereinafter the IEAP types are labelled according to electrode and membrane materials. Their fabrication and general features are as follows.

PtNaf is a typical water-based IPMC with Nafion® membrane and platinum electrodes. It contains mobile sodium cations while the anionic sulfonate groups are immobile and secured to the polymeric backbone. Although this material is intended for continuous work in water environment, the measurements of short duration can be carried out in air without having to consider the fluid dynamics or influence of solvent evaporation. This material is relatively fast, gains its maximal actuating amplitude in a second only, and relaxes back in about 10 seconds. Its working voltage is mostly limited by the electrochemical stability window of water. The particular samples were cut from the sheets of Muscle-sheet^{TM}, which were obtained from Biomimetics Inc. about ten years ago, but stored continuously in deionized water. Prior to the experiments, the samples were processed with hydrochloric acid and lithium hydroxide according to the instructions of the manufacturer.

CNaf is an IEAP that holds ionic polymer membrane with nanoporous carbon electrodes. It is prepared according to the direct assembly process (DAP). This fabrication method was originally proposed by Akle *et al*. in 2007 [38] and later enhanced by Palmre *et al*. [39]. The membrane of this IEAP is made of Nafion® 117. The electrolyte is IL, 1-ethyl-3-methylimidazolium trifluoromethanesulfonate (EMImTFS). Its electrodes are made of the high-surface-area nanoporous CDC, further covered with one or several layers of gold foils with the thickness of about 130 nm. The gold layer guarantees good electrical conductivity of the electrodes that in turn improves actuation speed, force, and provides effective voltage and current transfer all over the IEAP. This material produces considerable amplitude of bending in the hertz-range frequency. A comprehensive description about the fabrication process as well as the material properties of this IEAP is available in [39], referred to as the Carbon(1). The particular samples were fabricated onsite by Ms. Inga Põldsalu, in 2011.

CPvf is a new type of IEAP, which does not involve ionic polymer. Instead, a non-ionic PVdF(HFP) is combined with a woven fiberglass cloth forming a reinforced membrane. The CDC electrodes are spray-coated onto the membrane. Similar to the previous IEAP type, the conductivity of the electrodes is improved by a few layers of gold foil. The whole laminate is immersed in EMImTFS IL, which results in ionic system where both ions are mobile and participate in deforming the laminate. Spray-coating technique allows accurate control of the thickness of each layer. The particular sample, used in this thesis,

has rather thick (170 μm) electrodes and about 50 μm thick membrane, resulting in a total thickness of about 400 μm. The relatively thick electrodes increase the effective stiffness of the laminate and result in capacitance per area of IEAP laminate of more than 0.4 F cm^{-2}. The power density of this IEAP material is 2.6 kW dm^{-3} and maximum energy density is 7 Wh dm^{-3} (when charged up to 2 V). Both parameters are comparable to those of the commercially available EDLCs. The fiberglass cloth restricts the in plane expansion or contraction of both electrodes, and positions the neutral layer of bending exactly to the centroid of the laminate. Hence, while one of the electrodes is expanding the other is compressed. This improves the bending performance as well as the blocking force. The particular samples were fabricated onsite by Ms. Inna Baranova, in 2014.

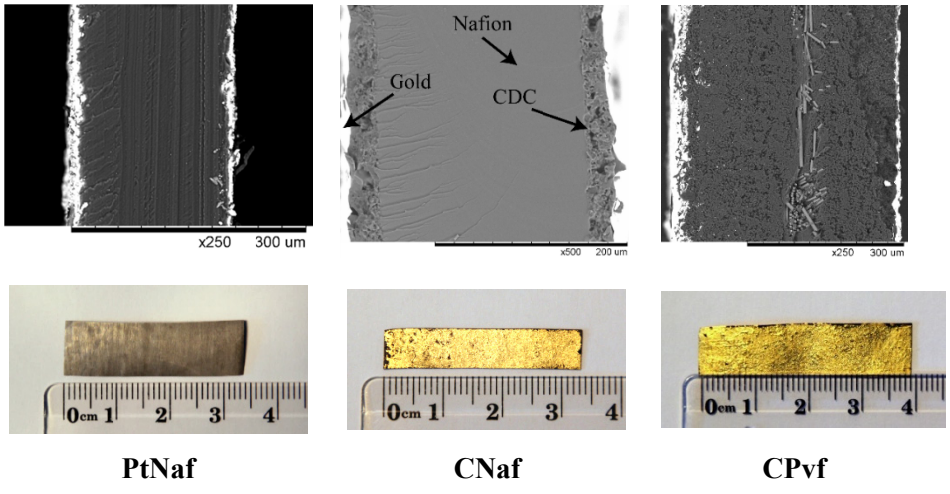

Figure 19. Scanning electron micrographs and optical images of **PtNaf**, **CNaf** and **CPvf** samples

The comparison of the optical and scanning electron micrographs of the three materials are given in figure 19. Here we must bring out that the two IEAP materials – **CNaf** and **CPvf** – are composed of identical IL and electrodes of identical carbon powder; the substantial difference is the material of the membrane: for **CNaf** it is an ionic polymer, while for **CPvf** it is a non-ionic polymer. Another significant difference is in the electrode to membrane ratio. The comparison of all three IEAP types is given in table 1.

Table 2. The comparison of the **PtNaf**, **CNaf** and **CPvf** IEAPs

	PtNaf	**CNaf**	**CPvf**
Additional current collector	none	gold foil	gold foil
Electrode material	platinum	CDC + Nafion®	CDC + PVdF(HFP)
Membrane	Nafion®	Nafion®	PVdF(HFP)
Membrane reinforcement	none	none	fiberglass cloth
IL/electrolyte solution	DI water + Na^+	EMImTFS	EMImTFS
Electrode thickness (each)	~15 μm	30 μm	170 μm
Membrane thickness	200 μm	200 μm	50 μm
Ratio of thickness of both electrodes to membrane thickness	0.15	0.3	6.8

5.2. Verification of the distributed electromechanical model

In this thesis, the validation of the distributed model is performed with the IEAPs **PtNaf** and **CNaf**, defined in subsection 5.1.

5.2.1. Experimental setup

Verifying a distributed model requires recording and analyzing time- and coordinate-dependent displacement of the IEAP actuator. This can be accomplished with vectored approach, which has been discussed in section 4.2.3. We set-up a continuous monitoring system using a CCD video camera (Dragonfly Express, Point Grey) that was connected to the LabVIEW image acquisition software through a FireWire interface. A custom-made software was prepared for generating step voltage signal and recording images synchronously. Since the maximum output current of National Instruments data acquisition hardware (PCI-6034) is not sufficient for high-capacity IEAP actuators, a current amplifier (HCB-20, HEKA) is added. The stored video frames are processed into discretized curvature along the length of the IEAP for each time instance forming a 2-dimensional matrix of curvature. The parameter fitting and comparison with experimentally obtained data was performed in MATLAB software with respect to equations (23)–(26). The conclusive schematic of the experimental setup together with the registered voltages are shown in figure 20.

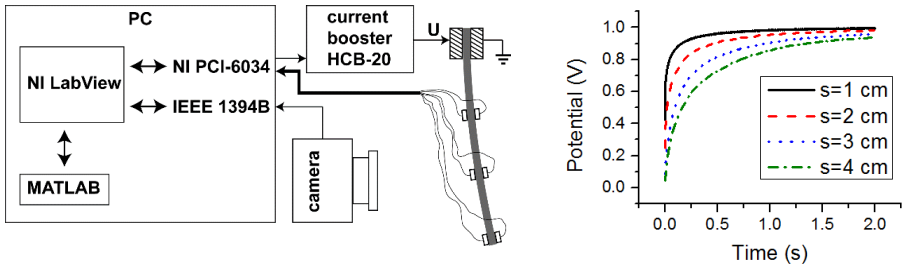

A **B**

Figure 20. A – experimental setup for distributed electromechanical model verification; B – the experimentally obtained potential differences along the lengthwise axis s of **PtNaf** sample with dimensions of 3 mm x 40 mm. The distance s is measured with respect to fixed clamps.

The total number of parameters of the proposed distributed model (see section 4.4) is six. Four of them (R, C, R_C, and R_{SS}) describe the electrical characteristics, and two – μ and λ – describe the electromechanical coupling and rate of relaxation, respectively. The parameter identification starts with determining the lengthwise electrode resistance R by two point or four point probe method. The rest of the electrical parameters can be identified by clamping the sample entirely between terminals and measuring current consumed by the IEAP during a step voltage excitation. This technique is previously described by Punning *et al.* in [103]. An alternative approach is to monitor the voltage propagation along the sample directly by attaching additional pairs of contacts as indicated in figure 20A. Since the PDE (22) describes the voltage distribution $v(s,t)$, it is natural to use the alternative approach and identify the model parameters relying on the actual voltage distribution measured from the actuator. Another benefit from direct voltage measurement is that the homogeneousness of electrical parameters along the IEAP laminate can be investigated. Finally, the recorded distributed curvature is used to find μ and λ from equation (26).

Conclusively, the parameter identification procedure is divided into 3 phases:

1. measurement of the electrode lengthwise resistance $R_e = R_a + R_b$ using four point probe method;
2. identification of C, R_C, and R_{SS} from direct distributed voltage measurement using parameter fitting;
3. identification of μ and λ from experimentally obtained distributed curvature using parameter fitting.

All parameters, except R, were identified by using differential evolution (DE) algorithm [107]. DE is a genetic algorithm for global optimization that is designed to solve problems with large parameter space. Compared to the gradient-based methods, DE does not assume continuous derivatives, is able to overcome local minimums, and suits well for optimizing against the noisy experimental

data. In this thesis, a sum of the squares of the errors between experimental and simulated data was chosen as a cost function to be minimized.

5.2.2. Results

The identified parameters for the IEAPs of type **PtNaf** and **CNaf** are presented in table 3. The results confirm that **CNaf** sample, which electrodes are covered with additional gold layer, shows better electrode conductivity along its length, when compared with **PtNaf**. The **CNaf** also has higher capacitance (0.13 F cm^{-2}), but is less efficient in terms of charge to curvature ratio. In fact, **PtNaf** is able to attain same curvature using 15 times less charge than that of required for **CNaf**.

Table 3. Identified parameters normalized with respect to the dimensions of the samples

	Dimensions (mm)	R_e $(\Omega\ sq^{-1})$	C $(mF\ cm^{-2})$	R_c $(\Omega\ cm^2)$	R_{ss} $(\Omega\ cm^2)$	α $(C^{-1}\ cm^{-1})$	λ (s^{-1})
PtNaf	45x3x0.24	4.5	19.7	3.0	42.9	29.5	0.29
CNaf	28x5x0.22	2.5	131	4.5	22.7	2.1	0.0029

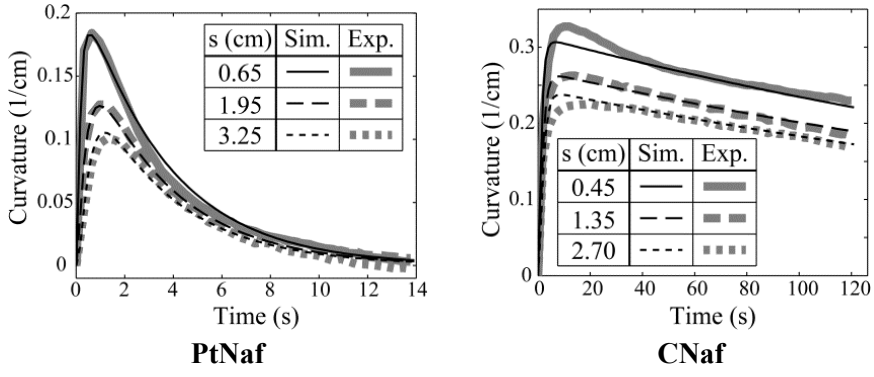

Figure 21. The comparison of simulated and measured bending of IEAPs with platinum and CDC electrodes

5.3. Effect of ambient environment on IEAPs

In this section, we demonstrate the functionality of the gray-box model presented in chapter 4.3.3 by investigating the effects of ambient environment on two carbon-based IEAPs – **CNaf** and **CPvf**. The actuation response as well as the electrical response of the two IEAP materials were investigated in three different environments, with respect to the Heaviside step input of various

potentials. The particular **CNaf** and **CPvf** samples analyzed in this section revealed notably lower conductivity in their thickness direction as compared to that of identified for samples in section 5.2.2. Therefore, in this section, the lengthwise voltage drop is negligible. For that reason, a distribute model is superfluous here and the simple model with two R–C branches (developed in 4.3.3) is used.

5.3.1. Specifications of the testing environments

The IEAP samples made of **CNaf** and **CPvf** materials were tested in three different environments, hereinafter referred as **Vacuum**, **Inert**, and **Air**.

Vacuum environment was realized with Hitachi TM3000 tabletop scanning electron microscope (SEM) equipped with electrical terminals in the investigation chamber. To suppress noise from electrical measurements as well as from captured images, the measurements were performed in charge reduction mode (chamber pressure is 50–60 Pa) at 15 kV excitation voltage. One input terminal of the sample was perpetually grounded to the chassis of the investigation chamber.

Inert is a controlled environment with extremely low water and oxygen content at normal barometric pressure. The Sci-Lab SG 1200/750 (Vigor Purification Tech. Inc.) glovebox was supplied with pure nitrogen (99.999 %, AGA, The Linde Group) gas. The concentrations of oxygen as well as water vapor were continuously monitored and maintained below 1 ppm.

Air is an ordinary ambient room environment. The experiments were conducted in a facility without air-conditioning equipment. Thus, the ambient conditions were most significantly determined by the outside weather. During the characterizations, the relative humidity and temperature levels nearby the experimental setup was in the range of 28–38 % and 24–29 °C, respectively.

5.3.2. Experimental setup

The electrical and mechanical characterization of the two IEAPs were performed with step input signals. The signal amplitudes (1.2 V, 2.0 V, and 2.5 V) were chosen so that they do not exceed the electrochemical stability window of the EMImTFS IL (4.1 V [18]), but definitely involve regions below and above the electrochemical stability window of water (1.23 V). With these voltage values, the possible influence of electrolysis of water in IEAPs can be clearly revealed.

The **CNaf** and **CPvf** samples with dimensions of 2 mm × 5 mm were attached between custom-made gold clamps and left intact during the whole experiment in all environments. This minimizes the impact of clamping pressure [108] and prevents fluctuations in contact resistance. The samples were tested in the following order: **Vacuum**, **Inert**, **Air**. Prior to applying the step input voltage, the inputs of the samples were held shorted for at least an hour to

discharge the sample. In all three environments, the voltages were applied in increasing order: 1.2 V, 2.0 V, 2.5 V.

The equipment used for the experiment was:

- the signal generation and current measurement were performed with the Compactstat potentiostat (Ivium Technologies);
- the bending was recorded with:
  a. **Vacuum –** the 1280 x 1040 px frames were recorded with the Hitachi TM3000 SEM equipment software;
  b. **Inert** and **Air** – the 1280 x 1024 px frames were recorded using an optical microscope, the DCM130 (Scopetek) USB camera, and LED backlight. The optical microscope magnification was adjusted so that the sample fits entirely into the sensor area and involves maximum number of pixels.

Using the distributed vector representation, discussed in section 4.2.3, the frames of both material types were analyzed with the tools that were developed in MATLAB (Mathsoft) and LabVIEW (National Instruments) programming environments. The distributed representation was also used to ensure that the constant curvature assumption is valid for each experiment.

5.3.3. Effect of humidity on electrical and mechanical parameters

The electrical currents of **CNaf** and **CPvf** samples in each tested environment at highest and lowest potentials are plotted side-by-side in figure 22. The nearly matching results in **Vacuum** and in **Inert** indicate that the impact of atmospheric pressure on electrical properties is negligible for these materials. Since the amplitude of the input signal is certainly in the electrochemical stability window of the IL, no additional effects to double-layer charging are observed. Contrary, in **Air**, both IEAPs exhibit severe changes depending on the potential and depending on their constituents. For **CPvf**, the current at 1.2 V in **Inert** and in **Air** (figure 22C) practically overlaps. It implies that low or moderate humidity has no impact on the electrical behavior of this type of IEAPs when actuated below the limit of water electrolysis. However, when the potential between the two electrodes exceeds the limit of water electrolysis (for example, at 2.5 V step input), the water in IEAP starts to decompose into oxygen (O_2) and hydrogen (H_2) gas, consuming an additional current (depicted in figure 22B and figure 22D).

At 1.2 V, according to our best knowledge, no faradaic processes take place in the investigated IEAP materials. Nevertheless, the long-term current consumption of **CNaf** is increased in **Air** environment by an order of magnitude (figure 22A), pointing out that changes in electrical parameters occur even below the threshold of water electrolysis. On the contrary, for **CPvf** (figure 22C), no distinctive humidity-dependency at 1.2 V was observed.

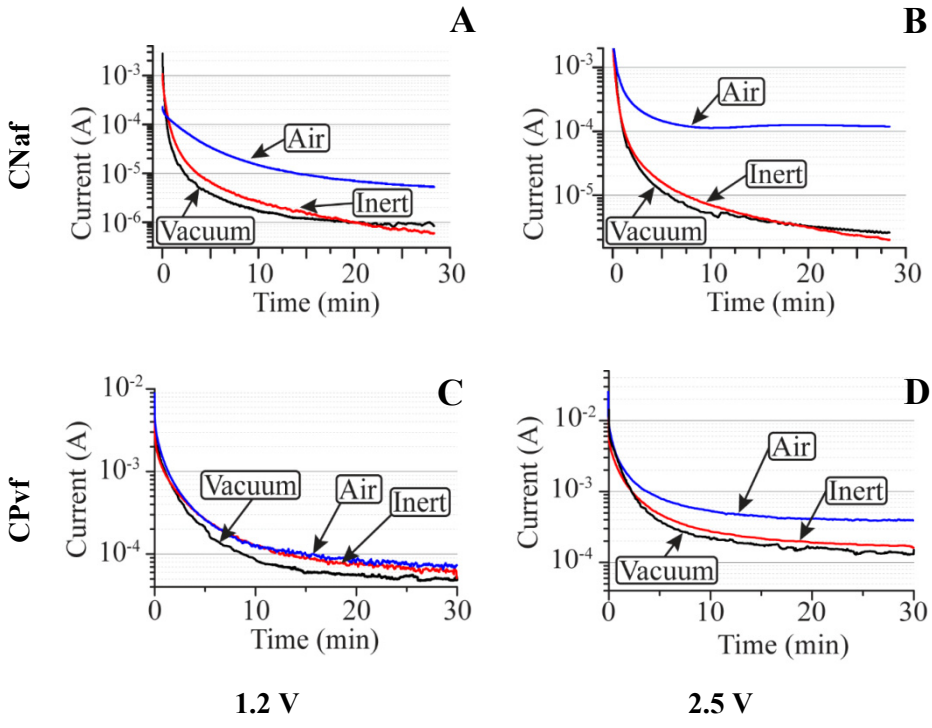

Figure 22. The electric current passing the IEAP actuators in the three different environments actuated with 1.2 V (A, C) and 2.5 V (B, D) step voltages

The summary given in figure 23 reveals the bending performance for both IEAP types in the three environments. A generic trend for both materials declares minor or no relaxation in **Vacuum** and **Inert** environments (figure 23A and figure 23C). However, the presence of water results in severe increase in the relaxation rate (figure 23B and figure 23D).

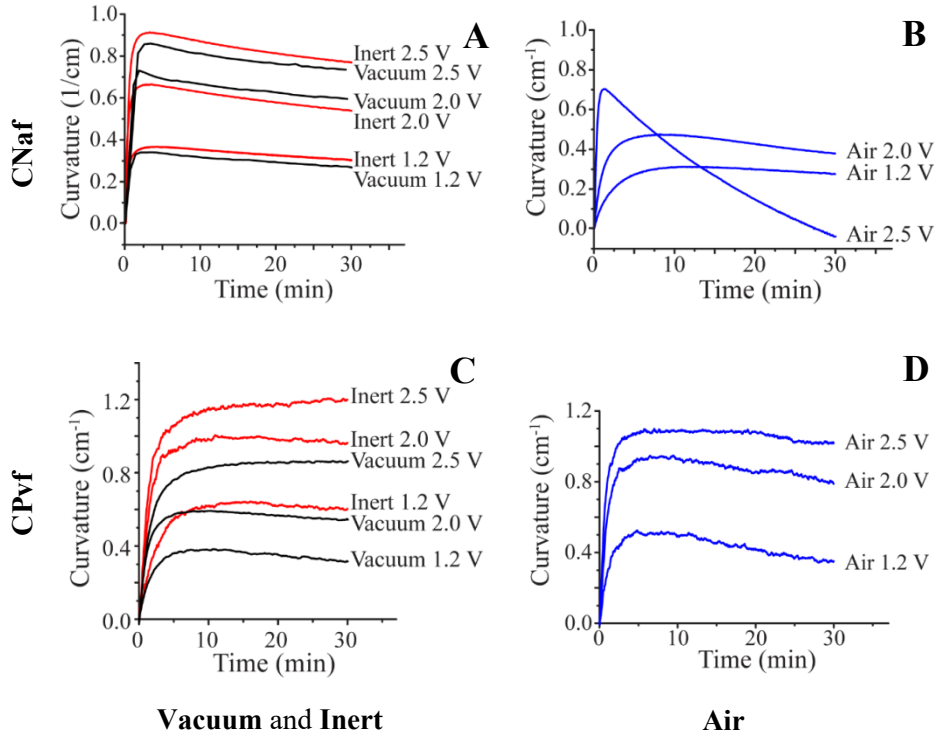

Figure 23. Experimentally obtained displacement of the two IEAP samples (A, C) – in **Vacuum** and **Inert** environments; (B, D) – in **Air** environment

5.3.4. Dynamical mechanical analysis

The electromechanical analysis revealed that the water has a severe impact on **CNaf** material while only minor impact on **CPvf** was observed. This motivated us to study the **CNaf** and its constituents in more detail. In particular, dynamical mechanical analysis (DMA) was performed with the three samples:

- dry Nafion® 117;
- Nafion® 117 immersed with EMImTFS IL;
- IEAP of type **CNaf**.

The experimental setup consisted of the DMA 242 (Artemis) equipment with DMA 242C and TASC 414/4 (NETZSCH) controllers. Since the IEAP actuators of interest operate in bending mode, it would be correct to investigate their mechanical properties using the same principles. Unfortunately, the sensitivity of the DMA 242 instrument is not sufficient for measuring samples with so low stiffness in bending mode and we had to switch over to tensile mode. The **CNaf** material is close to isotropic providing equivalent results of the two modes. This, however, does not apply for the **CPvf**, since its centroid is reinforced with

woven fiberglass cloth, which results in orders of magnitude lower stiffness for bending as compared to that of the axial. This is another reason why DMA studies of **CPvf** is attributed as a subject of future work.

The humidity in the DMA chamber was controlled with the modular humidity generator MHG32 (ProUmid) supplied with nitrogen (99.999 %, AGA, The Linde Group) gas. 5 mm wide samples were fixed in DMA instrument so that initial distance between the sample holder and the probe was 4.5 mm in all tests. The analysis was carried out at 1 Hz in tensile stress mode with constrained strain of 10 µm.

Concurrently with monitoring stresses and strains, the relative humidity around the sample was changed abruptly – from zero to 40 % and back to 0 %. Both levels were kept for 120 minutes. All samples were taken to stable state by pre-conditioning at 0 % humidity for at least 60 minutes. The obtained complex moduli of elasticity |E*| of the three samples are given in table 4, while the comparison of the relative change of samples is shown in figure 24.

Table 4. Complex moduli of elasticity of the samples before and after inducing humidity. Δ|E*| represents the relative increase of |E*| from t=0 to t=120.

Sample	**|E*| at t=0 (MPa)**	**|E*| at t=120 (MPa)**	**Δ|E*| (%)**
dry Nafion® 117	460	280	40
Nafion® 117 with EMImTFS IL	56	54	<5
CNaf	70	55	20

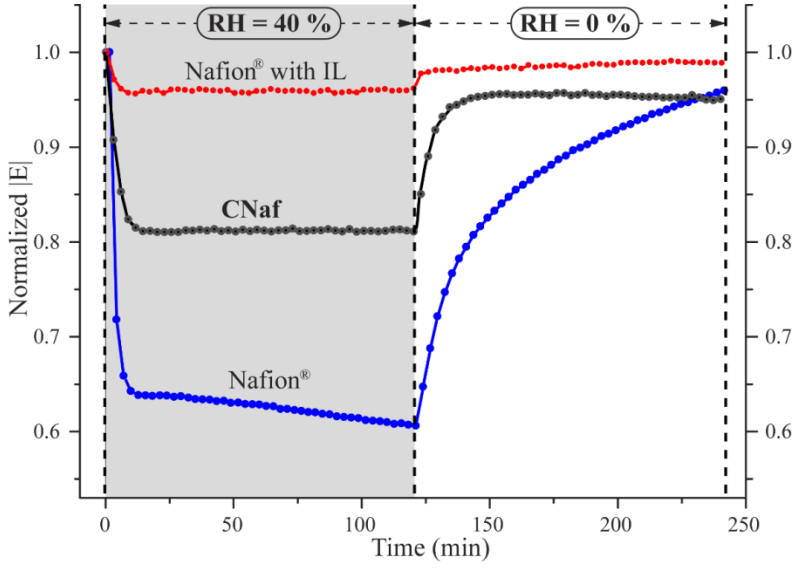

Figure 24. Normalized complex moduli of elasticity of the **CNaf** material, bare membrane, and membrane immersed in IL under rapidly changing humidity

The results bring evident that taking bare uncovered Nafion® from dry to humid (0 % to 40 % RH) environment decreased its complex modulus of elasticity by about 40 %. When changing from humid to dry environment, the full recovery of the bare Nafion® is considerably time-consuming. The low drying rate of bare Nafion® is delineated by Majsztrik *et al*.:" it takes more than a day for water absorption to be equilibrated" [101]. Impregnating Nafion® in IL lowers its |E*| by almost an order of magnitude. At the same time, the impact of the varying humidity on the |E*| becomes minor (less than 5 %) and the equilibrium is achieved shortly (5–10 minutes). Dependence of the **CNaf** IEAP sample on humidity is significantly higher (about 20 %); although, covering the IL-impregnated Nafion® with carbonaceous electrodes does not change the |E*| substantially. A possible explanation to this behavior is that during the last step of the fabrication process – hot pressing – a small amount of IL is expelled from the laminate. Now there is more room for water molecules to diffuse into the laminate; therefore, the IEAP responds to humidity more intensively. The carbonaceous electrode layers act as additional buffers, which slow down the diffusion of water towards the Nafion® membrane. Hence, taking the IEAP laminate from dry environment to humid, the equilibrium reaches in about 20 minutes.

5.3.5. Results and discussion

In order to compare the influence of each implicated environment to the electrical and mechanical properties of an IEAP, we can use the benefits of the gray-box model developed in section 4.3.3 and identify all parameters from the experimentally obtained data. Analogously to the verification of the distributed model, the parameter identification was performed at this time in multiple steps. First, the electrical parameters were found by fitting simulated current against the experimentally obtained curve. Secondly, with fixed electrical parameters, the two mechanical parameters were identified from the experimentally obtained curvature of the IEAP actuator. The DE fitting technique was used for both identification procedures. For either tested IEAP, a three by three by seven matrix of parameters was obtained (see table 5).

The curvature is proportional to the accumulated electric charge. Without taking into account the back-relaxation processes, the maximum bending curvature would be directly determined by the total charge stored in C_1 and C_2. For that reason, it is convenient to characterize the material with the summarized capacitance (C_1+C_2), which expresses the total charge, normalized with respect to input potential. The value of the initial peak of electric current of the equivalent circuit model is determined by R_1, R_2, and R_{ss} connected in parallel. The R_1 and R_2 in parallel ($R_1||R_2$) determine the instantaneous charging current, while R_{ss} describes the steady-state current consumption after the capacitors are fully charged to input voltage. All parameters are separately graphed in figure 26 to give an intuitive overview about the relations between the parameters, applied potential, and the environment.

Table 5. Fitted values of the electromechanical equivalent circuit

	Environment	Vacuum			Inert			Air		
	V_0 (V)	**1.2**	**2.0**	**2.5**	**1.2**	**2.0**	**2.5**	**1.2**	**2.0**	**2.5**
CNaf	R_1 $(\Omega\ cm^2)$	64.4	107.6	92.8	173.1	128.2	124.1	1544.9	521.4	158.1
	C_1 $(F\ cm^{-2})$	0.039	0.026	0.137	0.033	0.049	0.075	0.010	0.098	0.146
	R_2 $(\Omega\ cm^2)$	130.3	124.3	1533.7	316.2	305.8	694.7	844.1	2629.9	638.1
	C_2 $(F\ cm^{-2})$	0.10	0.13	0.06	0.11	0.10	0.08	0.22	0.13	0.17
	R_{ss} $(k\Omega\ cm^2)$	64.05	61.08	67.59	109.86	76.02	76.76	18.51	5.66	1.91
	R^2	0.996	0.996	0.999	0.994	0.996	0.993	0.996	0.999	0.996
	α $\left(C^{-1}cm^{-1}\right)$	24.62	26.56	17.57	21.50	22.15	23.14	12.46	13.88	12.28
	λ $\left(s^{-1}\right)$	9.4E-05	1.1E-04	9.4E-05	1.2E-04	1.4E-04	4.8E-05	1.6E-04	3.8E-04	1.8E-03
	R^2	0.941	0.990	0.940	0.990	0.995	0.994	0.985	0.948	0.957
CPvf	R_1 $(\Omega\ cm^2)$	37.6	35.4	34.3	35.3	38.6	37.8	23.4	20.7	19.6
	C_1 $(F\ cm^{-2})$	0.039	0.031	0.027	0.055	0.030	0.039	0.060	0.067	0.053
	R_2 $(\Omega\ cm^2)$	81.5	63.9	55.3	87.6	72.0	68.7	43.1	37.8	34.2
	C_2 $(F\ cm^{-2})$	1.22	1.44	1.63	1.56	1.35	1.46	1.94	1.87	1.90
	R_{ss} $(k\Omega\ cm^2)$	1.73	1.85	1.70	2.36	0.93	1.45	1.72	1.00	0.63
	R^2	0.951	0.973	0.984	0.961	0.973	0.971	0.973	0.962	0.962
	α $\left(C^{-1}cm^{-1}\right)$	1.97	2.06	2.02	4.33	4.74	4.31	3.02	3.41	3.07
	λ $\left(s^{-1}\right)$	1.8E-04	6.4E-05	0	8.5E-05	4.9E-06	0	2.8E-04	1.1E-04	6.0E-05
	R^2	0.990	0.993	0.952	0.975	0.990	0.971	0.974	0.982	0.964

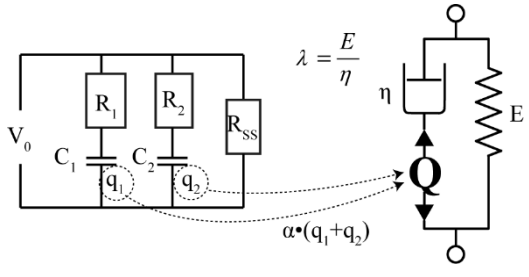

Figure 25. Electromechanical model of IEAP (a copy of figure 12B to improve the understanding of table 5)

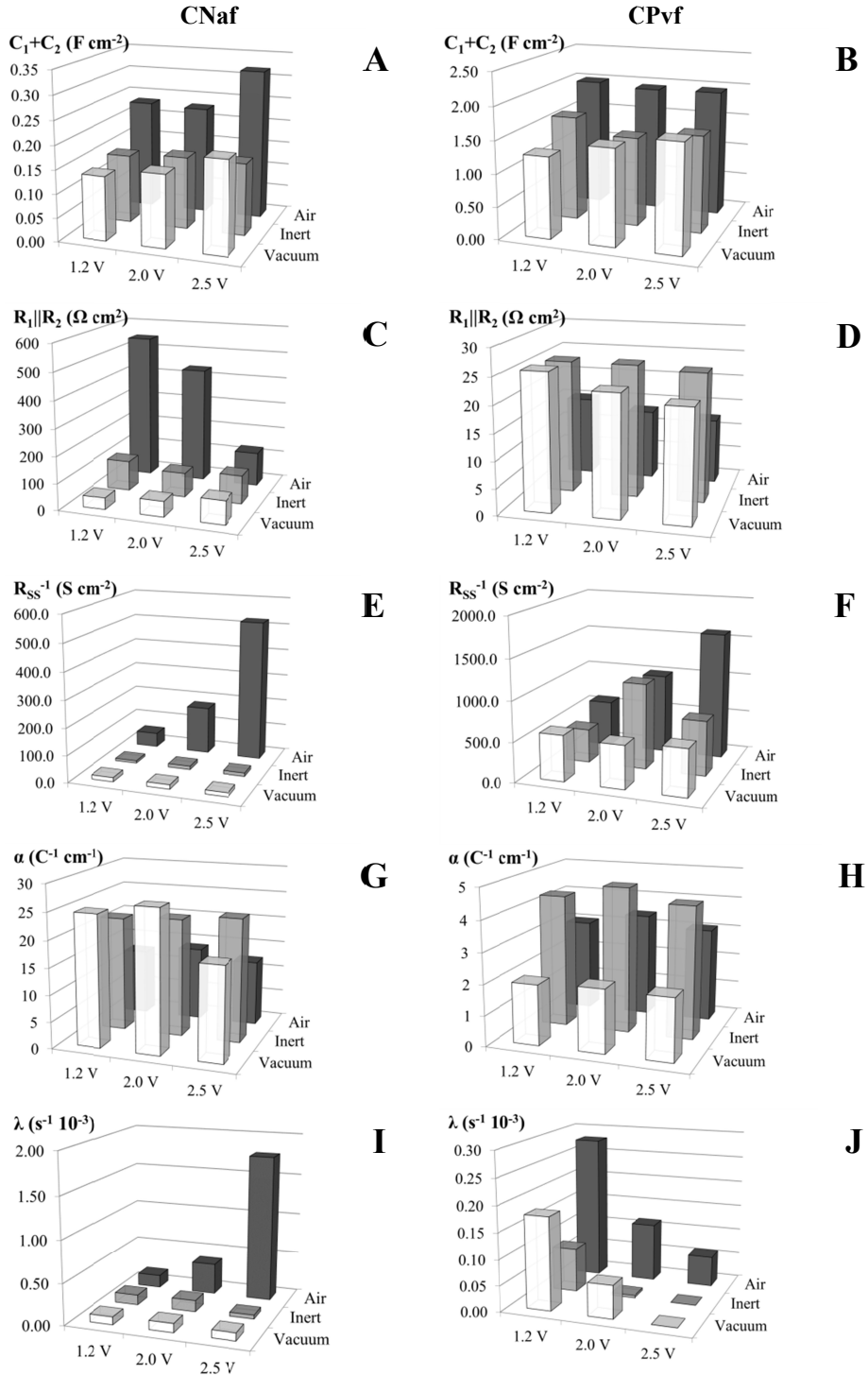

Figure 26. Comparison of the identified parameters

At first glance, the two IEAPs investigated in this section may seem similar – both of them contain the same electrode material, EMImTFS IL, and current collectors. On the other hand, the differences of **CNaf** and **CPvf** concern the used polymers, proportions of membrane thickness to electrode thicknesses, and manufacturing techniques (see table 2 in section 5.1). The too large number of differences prevents the thorough fundamental comparison of the two IEAP types. Nevertheless, the proposed gray-box model allows for IEAP comparison in a more generic level involving features that are important from engineering point of view. The analysis of **CNaf** parameters in **Air** brings forward the high value of $R_1||R_2$ that decreases with increasing potential (figure 26C). This effect can be a consequence of several processes, which all are depending on a common factor – water. The polymer used for **CNaf** membrane and for electrode binder is Nafion®, which contains anionic sulfonate groups. These groups make the Nafion® highly hydrophilic. The EMImTFS IL is hydrophilic as well. Since the studied carbon-based IEAPs are covered with gold foil, the water diffusion from the outermost electrode surfaces towards the IEAP core is limited, but not prevented due to the cracks in compact metal layer. The entering water expands the lattice and accelerates the water transport into the polymer network even more. Due to the Nafion® swelling, the electronic conductivity between the carbon particles decreases. On the other hand, the absorbed water decreases viscosity of the IL water mixture improving the diffusion rates and resulting in higher ionic conductivity. Therefore, the change in electronic conductivity of carbon particles is compensated by the opposed change of the ionic conductivity of IL, both of which are unified as $R_1||R_2$ in the model.

When the electrochemical stability window of water is exceeded, the water is being electrolyzed and removed from the IEAP in form of gaseous oxygen and hydrogen. This is an important aspect to consider while interpreting the model parameters because the above-mentioned trends are changed and the model parameters become disturbed. For potentials below the electrochemical stability window of water, C_1 and C_2 are uniquely identified as double-layer capacitances, but the figure 26A declares that for higher potentials (2.5 V), the total capacitance is increased. We believe that this increase is fictively caused by the added reversible and irreversible electrochemical processes related to water electrolysis, but is not separately modeled in this dissertation. The effect of electrochemical processes on steady-state resistance R_{SS} is highlighted in figure 26E.

As indicated in figure 23C and in figure 26H, in **Vacuum**, the electromechanical coupling coefficient α of **CPvf** has been reduced by approximately two times (for **CNaf** this effect does not occur). At the same time, all electrical parameters as well as the rate of relaxation remained nearly unchanged. It means that the same electric charge is not able to deform the material as much as in normal barometric conditions, and is registered as reduced bending performance. Recalling chapter 4.3.3, the coupling coefficient α is proportional to electrically induced bending moment and inversely proportional to stiffness.

From that, either the stiffness or the electrically induced bending moment or both of the quantities have changed in **Vacuum**.

The main difference between the two carbon-based IEAPs is the polymer. The Nafion® in **CNaf** becomes porous in water or IL due to swelling. Instead, the microporous structure of PVdF(HFP) in **CPvf** is formed during manufacturing possibly containing empty pores. We suspect that in **Vacuum** the **CPvf** polymer network collapses, which results in the increased stiffness of the IEAP laminate. Nevertheless, this aspect should be verified in future by carrying out additional force measurements in **Vacuum** environment.

6. SUMMARY

The actuation of the IEAP actuators is caused by the expansion and contraction of the separate viscoelastic layers of the multilayer material. Figuratively, the displacement is initiated from "inside" of the layers of the laminate, between the viscous and elastic threads of the polymer molecules network. The classical schemes of viscoelasticity – the Maxwell model, Kelvin-Voigt model, and the various combinations of the two – are unable to describe simultaneously the actuation and relaxation of the IEAP materials. To fulfill this gap, this dissertation presents a novel gray-box electromechanical model. It consists of traditional viscoelastic elements – spring and damper, but the motive force acts in a non-traditional way – between the spring and damper. The resulting electromechanical model is defined by simple PDE, which parameters can be identified experimentally.

Incorporation of a series of short entities of the developed lumped electromechanical model, results in a distributed model of the IEAP actuators. This assembly resembles a serial robotic manipulator with active joints powered according to our model of viscoelasticity. It takes into account the superposition principle and describes *inter alia* the back-relaxation of the actuators after their forced bending forward.

A criterion for choosing between the two models – lumped or distributed – is the ratio of lengthwise electrode conductivity to the conductivity across the material. If the lengthwise conductivity of the IEAP sample is excellent, then the simpler lumped model suits well enough. The distributed model should be chosen when the lengthwise electrode conductivity is comparable or lower with that of across the electrodes.

The identical experiments carried out in dry and humid ambient environments bring forward the twofold effect of ambient humidity to the IEAP actuators. On one hand, water molecules affect the electrical parameters – increase the ionic conductivity, lower electronic conductivity, and increase the apparent capacitance between the IL-permeated polymer membrane and the absorbing carbonaceous electrodes boundary. On the other hand, the presence of water lowers the viscosity of the IL and decreases the Young's modulus of the membrane. In less viscous system, the relaxation rate is increased. The water molecules associated with cations and anions of ionic liquid improve the ionic conductivity. The increased ionic conductivity accelerates the charging process and makes its steady state approaching faster. The softness of the swollen polymer membrane gives an additional contribution to the bending amplitude, but decreases the force applied by the actuator. The results are qualitatively summarized in the table 6.

Table 6. Summary of the results

	1.2V	**2.0V**	**2.5V**
Air	• no electrolysis of water • **CNaf**: minor back-relaxation; • **CPvf**: minor back-relaxation; • large time constant value	• electrolysis of water • **CNaf**: moderate back-relaxation • **CPvf**: minor back-relaxation	• intensive electrolysis of water • **CNaf**: intense back-relaxation • **CPvf**: minor back-relaxation • small time constant value
Inert and **Vacuum**	• no electrolysis of water • **CNaf**: minor back-relaxation • **CPvf**: minor back-relaxation • low steady state current • small time constant value		

The most remarkable outcome of the current work is the observation that the back-relaxation rate of the IEAPs with carbonaceous electrodes is negligible in the two dry environments – in **Vacuum** and in **Inert** environment. Comparison of the two IEAP types with ionic polymer membrane and non-ionic polymer membrane demonstrates convincingly that the source of back-relaxation is the effect of ambient humidity on the ionic polymer.

7. SUMMARY IN ESTONIAN

Ioonsete elektroaktiivsete polümeersete täiturite tagasivajumise modelleerimine ja iseloomustamine

Ioonsed elektroaktiivsed polümeerid (IEAP) on arukad komposiitmaterjalid, mille põhiosadeks on elektroodid, elektroode eraldav polümeermembraan ning elektrolüüt. Kui elektroodidele rakendada elektripinge, paigutuvad ioonid ümber moodustades elektroodi ja ioonjuhtiva faasi piirpinnale elektrilise kaksikkihi. Selle tulemusena tekib laminaadis kihiti erinev rõhujaotus, mistõttu kogu laminaat tõmbub kõveraks. IEAP materjalide elektriline käitumine on kirjeldatav hajusate elektriliste ekvivalentskeemidega, mis võimaldavad lihtsustatult modelleerida elektripinge ja laengu levikut piki IEAP materjali sõltuvalt ajast. Üldiselt on IEAP-s salvestunud laeng ja tekkinud deformatsioon proportsionaalselt seotud, kuid see kehtib vaid väikeste painete ja kiirete sisendsignaali muutuste korral. Uurides ühikastme elektrisignaali mehaanilist kostet, näeme, et materjali laadides laminaadi kõverus kasvab vastavalt laengule, kuid sellele järgneb aeglasem materjali tagasivajumine algasendi suunas. Tagasivajumine leiab aset olenemata sellest, et materjal ise jääb elektriliselt laetuks. Selline käitumine on olemuselt sarnane polümeersete materjalide jõu mõjul voolamisele ehk roomamisele, mida klassikaliselt kirjeldatakse viskoelastsete mudelitega (*Kelvin-Voigt*, *Maxwell*, *standard linear solid*, jne). Kuna need süsteemid kirjeldavad olukorda, kus jõu rakendamisel tekkiv elastne deformatsioon ja sellele järgnev roomamine on samasuunalised, ei sobi need oma algkujul IEAP liigutuse kirjeldamiseks.

Käesolevas väitekirjas esitletakse uudset elektromehaanilist mudelit, mis kirjeldab IEAP tagasivajumist kasutades standardseid viskoelastseid primitiive nagu vedru ja amortisaator. Mudeli parameetrid on eskaleeruvad ning tuvastatavad lihtsatest eksperimentaalsetest mõõtmistest. Seetõttu omab doktoritöös esitletud mudel märkimisväärset rolli eelkõige IEAP materjalide iseloomustamisel ja kvantitatiivsel võrdlemisel, aga on samatähtis IEAP-de tööpõhimõtete selgitamisel ja vajalike juhtalgoritmide arendamisel.

Väitekirja peatükis 4.4 kombineeritakse tagasivajumist kirjeldav mehaaniline mudel hajusa elektrimudeliga, mis võtab arvesse elektripinge ebaühtlast jaotust IEAP materjalis. Selline lähenemine võimaldab kirjeldada IEAP materjale, mille elektroodide pikisuunaline juhtivus on samas suurusjärgus või väiksem kui laminaadi paksuse suunas. Hajusat elektromehaanilist mudelit võib ette kujutada kui mitmete lülidega robotmanipulaatorit, mille iga lüli põhjustab elektriliselt indutseeritud paindemomenti vastavalt laetuse astmele selles kohas. Mehaaniline tagasivajumise mudel võimaldab arvesse võtta, et elektriliselt indutseeritud paindemomendi ja seega kogu materjali kõverus on ajas hääbuv ja sõltub laadimise ajaloost.

Käesoleva doktoritöö eksperimentaalses osas kontrolliti kõigepealt elektromehaanilise hajusmudeli paikapidavust erinevate IEAP materjaliga. Seejärel demonstreeriti lihtsustatud mudeli eeliseid, et analüüsida kahe karbiidset pärit-

olu süsinikelektroodidega IEAP materjalide tagasivajumist erinevates keskkondades: vaakumis, inertgaasi keskkonnas ja niiskes õhus. Mõlema materjali elektromehaanilist käitumist uuriti astmesignaali rakendamisel igas keskkonnas kolmel sisendpingel: 1,2 V; 2,0 V; 2,5 V.

Antud töö eksperimentaalse osa kõige olulisem järeldus on, et süsinikelektroodidega IEAP materjalide tagasivajumise kiirus on nii vaakumis kui ka inertgaasi keskkonnas tühiselt väike. Võrreldes ioonpolümeeriga ja mitte-ioonpolümeeriga IEAP materjale kuivas ja niiskes keskkonnas näitab selgelt, et tagasivajumise intensiivsus on otseselt seotud niiskuse mõjust ioonpolümeerile. See seab piirangud niisketes keskkondades töötamisel, kuid kinnitab väitekirjas uuritud materjalide sobivust näiteks kosmosetehnoloogia valdkonnas.

8. REFERENCES

[1] Leo D J 2007 *Engineering Analysis of Smart Material Systems* (Hoboken, NJ, USA: John Wiley & Sons, Inc.)

[2] Bar-Cohen Y 2004 *Electroactive Polymer (EAP) Actuators as Artificial Muscles: Reality, Potential, and Challenges* (SPIE Press)

[3] Huxley A F and Niedergerke R 1954 Structural Changes in Muscle During Contraction: Interference Microscopy of Living Muscle Fibres *Nature* **173** 971–3

[4] Must I, Kaasik F, Põldsalu I, Mihkels L, Johanson U, Punning A and Aabloo A 2015 Ionic and Capacitive Artificial Muscle for Biomimetic Soft Robotics *Adv. Eng. Mater.* **17** 84–94

[5] Kaasik F, Must I, Lust E, Jürgens M, Presser V, Punning A, Temmer R, Kiefer R and Aabloo A 2014 In situ measurements with CPC micro-actuators using SEM *Proc. of SPIE* vol 9056 p 90562B

[6] Guo S, Fukuda T, Kosuge K, Arai F, Oguro K and Negoro M 1994 Micro catheter system with active guide wire-structure, experimental results and characteristic evaluation of active guide wire catheter using ICPF actuator *1994 5th International Symposium on Micro Machine and Human Science Proceedings* p 191

[7] Bahramzadeh Y and Shahinpoor M 2012 Ionic Polymer-Metal Composites (IPMCs) as dexterous manipulators and tactile sensors for minimally invasive robotic surgery *Proc. of SPIE* vol 8340 p 83402O – 7

[8] Sadeghipour K, Salomon R and Neogi S 1992 Development of a novel electrochemically active membrane and "smart" material based vibration sensor/ damper *Smart Mater. Struct.* **1** 172–9

[9] Bandopadhya D, Bhattacharya B and Dutta A 2007 An active vibration control strategy for a flexible link using distributed ionic polymer metal composites *Smart Mater. Struct.* **16** 617

[10] Shahinpoor M and Kim K J 2001 Ionic polymer-metal composites: I. Fundamentals *Smart Mater. Struct.* **10** 819

[11] Punning A, Must I, Johanson U and Aabloo A 2015 Thermal behavior of ionic electroactive polymer actuators *Proc. of SPIE* vol 9430 p 94300E

[12] Park K, Yoon M-K, Lee S, Choi J and Thubrikar M 2010 Effects of electrode degradation and solvent evaporation on the performance of ionic-polymer–metal composite sensors *Smart Mater. Struct.* **19** 075002

[13] Bennett M D and Leo D J 2004 Ionic liquids as stable solvents for ionic polymer transducers *Sens. Actuators Phys.* **115** 79–90

[14] Dean J A 1998 *Lange's Handbook of Chemistry* (New York: McGraw-Hill)

[15] Kothera C, Leo D and Robertson L 2003 Hydration and Control Assessment of Ionic Polymer Actuators *44th AIAA/ASME/ASCE/AHS/ASC Structures, Structural Dynamics, and Materials Conference* (American Institute of Aeronautics and Astronautics) p 1441

[16] Wang J, Xu C, Taya M and Kuga Y 2007 A Flemion-based actuator with ionic liquid as solvent *Smart Mater. Struct.* **16** S214

[17] Nemat-Nasser S and Zamani S 2003 Experimental study of Nafion- and Flemion-based ionic polymer metal composites (IPMCs) with ethylene glycol as solvent *Proc. of SPIE* vol 5051 pp 233–44

[18] Zhang S, Sun N, He X, Lu X and Zhang X 2006 Physical Properties of Ionic Liquids: Database and Evaluation *J. Phys. Chem. Ref. Data* **35** 1475–517

[19] Plechkova N V and Seddon K R 2007 Applications of ionic liquids in the chemical industry *Chem. Soc. Rev.* **37** 123–50
[20] Mohammad A and Inamuddin D 2012 *Green Solvents II* (Dordrecht: Springer Netherlands)
[21] Hamlen R P, Kent C E and Shafer S N 1965 Electrolytically Activated Contractile Polymer *Nature* **206** 1149–50
[22] Osada Y and Hasebe M 1985 Electrically Activated Mechanochemical Devices Using Polyelectrolyte Gels *Chem. Lett.* **14** 1285–8
[23] De Rossi D E, Chiarelli P, Buzzigoli G, Domenici C and Lazzeri L 1985 Contractile behavior of electrically activated mechanochemical polymer actuators. *ASAIO Trans* **32** 157–62
[24] Kishi R and Osada Y 1989 Reversible volume change of microparticles in an electric field *J. Chem. Soc. Faraday Trans. 1 Phys. Chem. Condens. Phases* **85** 655–62
[25] Grimshaw P E, Nussbaum J H, Grodzinsky A J and Yarmush M L 1990 Kinetics of electrically and chemically induced swelling in polyelectrolyte gels *J. Chem. Phys.* **93** 4462–72
[26] Caldwell D G and Taylor P M 1990 Chemically stimulated pseudo-muscular actuation *Int. J. Eng. Sci.* **28** 797–808
[27] Shahinpoor M 1992 Conceptual design, kinematics and dynamics of swimming robotic structures using ionic polymeric gel muscles *Smart Mater. Struct.* **1** 91
[28] Rossi D D, Suzuki M, Osada Y and Morasso P 1992 Pseudomuscular Gel Actuators for Advanced Robotics *J. Intell. Mater. Syst. Struct.* **3** 75–95
[29] Tadokoro S, Fuji S, Fushimi M, Kanno R, Kimura T, Takamori T and Oguro K 1998 Development of a distributed actuation device consisting of soft gel actuator elements *1998 IEEE International Conference on Robotics and Automation* vol 3 pp 2155–60
[30] Segalman D J, Witkowski W R, Adolf D B and Shahinpoor M 1992 Theory and application of electrically controlled polymeric gels *Smart Mater. Struct.* **1** 95
[31] Fedkiw P S and Her W-H 1989 An Impregnation-Reduction Method to Prepare Electrodes on Nafion SPE *J. Electrochem. Soc.* **136** 899–900
[32] Shahinpoor M, Bar-Cohen Y, Simpson J O and Smith J 1998 Ionic polymer-metal composites (IPMCs) as biomimetic sensors, actuators and artificial muscles - a review *Smart Mater. Struct.* **7** R15
[33] Kanno R, Tadokoro S, Takamori T, Hattori M and Oguro K 1996 Linear approximate dynamic model of ICPF (ionic conducting polymer gel film) actuator *Proceedings of IEEE International Conference on Robotics and Automation* vol 1 pp 219–25
[34] Oguro K, Kawami Y and Takenaka H 1992 Bending of an Ion-Conducting Polymer Film-Electrode Composite by an Electric Stimulus at Low Voltage *Trans J. Micromachine Soc.* **5** 27–30
[35] Baughman R H, Cui C, Zakhidov A A, Iqbal Z, Barisci J N, Spinks G M, Wallace G G, Mazzoldi A, Rossi D D, Rinzler A G, Jaschinski O, Roth S and Kertesz M 1999 Carbon Nanotube Actuators *Science* **284** 1340–4
[36] Biso M and Ricci D 2009 Multi-walled carbon nanotubes plastic actuator *Phys. Status Solidi B* **246** 2820–3
[37] Akle B J, Bennett M D, Leo D J, Wiles K B and McGrath J E 2007 Direct assembly process: a novel fabrication technique for large strain ionic polymer transducers *J. Mater. Sci.* **42** 7031–41

[38] Akle B J, Bennett M D and Leo D J 2006 High-strain ionomeric–ionic liquid electroactive actuators *Sens. Actuators Phys.* **126** 173–81
[39] Palmre V, Brandell D, Mäeorg U, Torop J, Volobujeva O, Punning A, Johanson U, Kruusmaa M and Aabloo A 2009 Nanoporous carbon-based electrodes for high strain ionomeric bending actuators *Smart Mater. Struct.* **18** 095028
[40] Palmre V, Lust E, Jänes A, Koel M, Peikolainen A-L, Torop J, Johanson U and Aabloo A 2011 Electroactive polymer actuators with carbon aerogel electrodes *J. Mater. Chem.* **21** 2577–83
[41] Torop J, Kaasik F, Sugino T, Aabloo A and Asaka K 2010 Electromechanical characteristics of actuators based on carbide-derived carbon *Proc. of SPIE* vol 7642 p 76422A – 7
[42] Terasawa N, Ono N, Hayakawa Y, Mukai K, Koga T, Higashi N and Asaka K 2011 Effect of hexafluoropropylene on the performance of poly(vinylidene fluoride) polymer actuators based on single-walled carbon nanotube–ionic liquid gel *Sens. Actuators B Chem.* **160** 161–7
[43] Terasawa N, Hayashi Y, Koga T, Higashi N and Asaka K 2014 High-performance polymer actuators based on poly(ethylene oxide) and single-walled carbon nanotube–ionic liquid-based gels *Sens. Actuators B Chem.* **202** 382–7
[44] Green O, Grubjesic S, Lee S and Firestone M A 2009 The Design of Polymeric Ionic Liquids for the Preparation of Functional Materials *Polym. Rev.* **49** 339–60
[45] Naoko Fujiwara K A 2000 Preparation of Gold−Solid Polymer Electrolyte Composites As Electric Stimuli-Responsive Materials *Chem. Mater.* **12** 1750–4
[46] Oguro K, Fujiwara N, Asaka K, Onishi K and Sewa S 1999 Polymer electrolyte actuator with gold electrodes *Proc. of SPIE* vol 3669 pp 64–71
[47] Kim S-M and Kim K J 2008 Palladium buffer-layered high performance ionic polymer–metal composites *Smart Mater. Struct.* **17** 035011
[48] Kobayashi T and Omiya M 2012 Deformation behaviors of ionic-polymer–metal composite actuator with palladium electrodes for various solvents, temperatures, and frequencies *Smart Mater. Struct.* **21** 105031
[49] Shahinpoor M and Kim K J 2000 The effect of surface-electrode resistance on the performance of ionic polymer-metal composite (IPMC) artificial muscles *Smart Mater. Struct.* **9** 543
[50] Uchida M and Taya M 2001 Solid polymer electrolyte actuator using electrode reaction *Polymer* **42** 9281–5
[51] Johanson U, Mäeorg U, Sammelselg V, Brandell D, Punning A, Kruusmaa M and Aabloo A 2008 Electrode reactions in Cu–Pt coated ionic polymer actuators *Sens. Actuators B Chem.* **131** 340–6
[52] Pugal D, Jung K, Aabloo A and Kim K J 2010 Ionic polymer–metal composite mechanoelectrical transduction: review and perspectives *Polym. Int.* **59** 279–89
[53] Torop J, Arulepp M, Leis J, Punning A, Johanson U, Palmre V and Aabloo A 2009 Nanoporous Carbide-Derived Carbon Material-Based Linear Actuators *Materials* **3** 9–25
[54] Terasawa N, Ono N, Mukai K, Koga T, Higashi N and Asaka K 2012 High performance polymer actuators based on multi-walled carbon nanotubes that surpass the performance of those containing single-walled carbon nanotubes: Effects of ionic liquid and composition *Sens. Actuators B Chem.* **163** 20–8
[55] Kaasik F, Torop J, Peikolainen A-L, Koel M and Aabloo A 2011 Carbon aerogel based electrode material for EAP actuators *Proc. of SPIE* vol 7976 p 79760O
[56] Im K H and Choi H 2014 Electroactive polymer actuator based on a reduced graphene electrode *J. Korean Phys. Soc.* **64** 623–6

[57] Kim S-M, Tiwari R and Kim K J 2011 A Novel Ionic Polymer Metal ZnO Composite (IPMZC) *Sensors* **11** 4674–87
[58] Long Y-Z, Li M-M, Gu C, Wan M, Duvail J-L, Liu Z and Fan Z 2011 Recent advances in synthesis, physical properties and applications of conducting polymer nanotubes and nanofibers *Prog. Polym. Sci.* **36** 1415–42
[59] Temmer R 2014 *Electrochemistry and novel applications of chemically synthesized conductive polymer electrodes* Thesis (Tartu: University of Tartu)
[60] Nemat-Nasser S and Wu Y 2003 Tailoring actuation of ionic polymer metal composites through cation combination *Proc. of SPIE* vol 5051 pp 245–53
[61] Wang J, Xu C, Taya M and Kuga Y 2006 Mechanical stability optimization of Flemion-based composite artificial muscles by use of proper solvent *J. Mater. Res.* **21** 2018–22
[62] Kikuchi K, Miwa M and Tsuchitani S 2008 Evaluation of basic operating characteristics of ion conductive polymer actuator using ionic liquid *SICE Annual Conference, 2008* pp 1092–5
[63] Lee J-W, Hong S M and Koo C M 2014 High-performance polymer ionomer–ionic liquid membrane IPMC actuator *Res. Chem. Intermed.* **40** 41–8
[64] Plaado M, Kaasik F, Valner R, Lust E, Saar R, Saal K, Peikolainen A-L, Aabloo A and Kiefer R 2015 Electrochemical actuation of multiwall carbon nanotube fiber with embedded carbide-derived carbon particles *Carbon* **94** 911–8
[65] Yang W, Choi H, Choi S, Jeon M and Lee S-Y 2012 Carbon nanotube–graphene composite for ionic polymer actuators *Smart Mater. Struct.* **21** 055012
[66] Nemat-Nasser S and Wu Y 2003 Comparative experimental study of ionic polymer–metal composites with different backbone ionomers and in various cation forms *J. Appl. Phys.* **93** 5255–67
[67] Sugino T, Kiyohara K, Takeuchi I, Mukai K and Asaka K 2009 Actuator properties of the complexes composed by carbon nanotube and ionic liquid: The effects of additives *Sens. Actuators B Chem.* **141** 179–86
[68] Gennes P G de, Okumura K, Shahinpoor M and Kim K J 2000 Mechanoelectric effects in ionic gels *Europhys. Lett. EPL* **50** 513–8
[69] Nemat-Nasser S and Li J Y 2000 Electromechanical response of ionic polymer-metal composites *J. Appl. Phys.* **87** 3321
[70] Tadokoroa S, Yamagamia S, Takamoria T and Oguro K 2000 Modeling of Nafion-Pt composite actuators (ICPF) by ionic motion *Proc. of SPIE* vol 3987 pp 92–102
[71] Asaka K and Oguro K 2000 Bending of polyelectrolyte membrane platinum composites by electric stimuli: Part II. Response kinetics *J. Electroanal. Chem.* **480** 186–98
[72] Park J K, Jones P J, Sahagun C, Page K A, Hussey D S, Jacobson D L, Morgan S E and Moore R B 2010 Electrically stimulated gradients in water and counterion concentrations within electroactive polymer actuators *Soft Matter* **6** 1444–52
[73] Bennett M D, Leo D J, Wilkes G L, Beyer F L and Pechar T W 2006 A model of charge transport and electromechanical transduction in ionic liquid-swollen Nafion membranes *Polymer* **47** 6782–96
[74] Li J, Wilmsmeyer K G, Hou J and Madsen L A 2009 The role of water in transport of ionic liquids in polymeric artificial muscle actuators *Soft Matter* **5** 2596–602
[75] Imaizumi S, Kato Y, Kokubo H and Watanabe M 2012 Driving Mechanisms of Ionic Polymer Actuators Having Electric Double Layer Capacitor Structures *J. Phys. Chem. B* **116** 5080–9

[76] Akle B J, Leo D J, Hickner M A and McGrath J E 2005 Correlation of capacitance and actuation in ionomeric polymer transducers *J. Mater. Sci.* **40** 3715–24
[77] Kikuchi K and Tsuchitani S 2009 Nafion®-based polymer actuators with ionic liquids as solvent incorporated at room temperature *J. Appl. Phys.* **106** 053519
[78] Kim D and Kim K J 2007 Can we overcome the relaxation of ionic polymer-metal composites? *Proc. of SPIE* vol 6524 p 65240A – 11
[79] Fleming M J, Kim K J and Leang K K 2012 Mitigating IPMC back relaxation through feedforward and feedback control of patterned electrodes *Smart Mater. Struct.* **21** 085002
[80] Shoji E and Hirayama D 2007 Effects of Humidity on the Performance of Ionic Polymer−Metal Composite Actuators: Experimental Study of the Back-Relaxation of Actuators *J. Phys. Chem. B* **111** 11915–20
[81] Newbury K 2002 *Characterization, Modeling, and Control of Ionic Polymer Transducers by Characterization, Modeling, and Control of Ionic Polymer Transducers* (Virginia Polytechnic Institute and State University)
[82] Bao X, Bar-Cohen Y and Lih S-S 2002 Measurements and macro models of ionomeric polymer-metal composites (IPMC) *Proc. of SPIE* vol 4695 pp 220–7
[83] Xue T and Longwell R B 1991 Mass transfer in Nafion membrane systems: Effects of ionic size and charge on selectivity *J. Membr. Sci.* **58** 175–89
[84] Akle B J and Leo D J 2013 Softening and heating effects in ionic polymer transducers: An experimental investigation *J. Intell. Mater. Syst. Struct.* **24** 1266–77
[85] Nemat-Nasser S 2002 Micromechanics of actuation of ionic polymer-metal composites *J. Appl. Phys.* **92** 2899
[86] Yagasaki K and Tamagawa H 2004 Experimental estimate of viscoelastic properties for ionic polymer-metal composites *Phys. Rev. E* **70** 052801
[87] Hao L, Sun Z, Li Z, Su Y and Gao J 2012 A novel adaptive force control method for IPMC manipulation *Smart Mater. Struct.* **21** 075016
[88] Kikuchi K, Sakamoto T, Tsuchitani S and Asaka K 2011 Comparative study of bending characteristics of ionic polymer actuators containing ionic liquids for modeling actuation *J. Appl. Phys.* **109** 073505
[89] Must I, Vunder V, Kaasik F, Põldsalu I, Johanson U, Punning A and Aabloo A 2014 Ionic liquid-based actuators working in air: The effect of ambient humidity *Sens. Actuators B Chem.* **202** 114–22
[90] Kruusamäe K, Mukai K, Sugino T and Asaka K 2015 Electroactive Shape-Fixing of Bucky-Gel Actuators *IEEEASME Trans. Mechatron.* **20** 1108–16
[91] Firoozbakhsh K, Shahinpoor M and Shavandi M 1998 Mathematical modeling of ionic interactions and deformation in ionic polymer-metal composite artificial muscles *Proc. of SPIE* vol 3323 pp 577–87
[92] Yamaue T, Mukai H, Asaka K and Doi M 2005 Electrostress Diffusion Coupling Model for Polyelectrolyte Gels *Macromolecules* **38** 1349–56
[93] Pugal D, Kim K J and Aabloo A 2011 An explicit physics-based model of ionic polymer-metal composite actuators *J. Appl. Phys.* **110** 084904
[94] Martinez M and Lumia R 2013 Distributed force simulation for arbitrarily shaped IPMC actuators *Smart Mater. Struct.* **22** 075024
[95] Pugal D, Solin P, Aabloo a and Kim K J 2013 IPMC mechanoelectrical transduction: its scalability and optimization *Smart Mater. Struct.* **22** 125029
[96] Pugal D, Solin P, Kim K J and Aabloo a. 2014 hp-FEM electromechanical transduction model of ionic polymer–metal composites *J. Comput. Appl. Math.* **260** 135–48

[97] Ruiz S, Mead B, Palmre V, Kim K J and Yim W 2015 A cylindrical ionic polymer-metal composite-based robotic catheter platform: modeling, design and control *Smart Mater. Struct.* **24** 015007
[98] Pei Q and Inganäs O 1992 Electrochemical applications of the bending beam method. 1. Mass transport and volume changes in polypyrrole during redox *J. Phys. Chem.* **96** 10507–14
[99] Punning A, Vunder V, Must I, Johanson U, Anbarjafari G and Aabloo A 2016 In situ scanning electron microscopy study of strains of ionic electroactive polymer actuators *J. Intell. Mater. Syst. Struct.* **27** 1061–74
[100] Liu Y, Zhao R, Ghaffari M, Lin J, Liu S, Cebeci H, de Villoria R G, Montazami R, Wang D, Wardle B L, Heflin J R and Zhang Q M 2012 Equivalent circuit modeling of ionomer and ionic polymer conductive network composite actuators containing ionic liquids *Sens. Actuators Phys.* **181** 70–6
[101] Majsztrik P W, Bocarsly A B and Benziger J B 2008 Viscoelastic Response of Nafion. Effects of Temperature and Hydration on Tensile Creep *Macromolecules* **41** 9849–62
[102] Roscoe R 1950 Mechanical Models for the Representation of Visco-Elastic Properties *Br. J. Appl. Phys.* **1** 171
[103] Punning A, Johanson U, Anton M, Aabloo A and Kruusmaa M 2009 A Distributed Model of Ionomeric Polymer Metal Composite *J. Intell. Mater. Syst. Struct.* **20** 1711–24
[104] Kruusamäe K, Punning A and Aabloo A 2012 Electrical model of a carbon-polymer composite (CPC) collision detector. *Sensors* **12** 1950–66
[105] Heaviside O 2011 *Electromagnetic Theory* (Cambridge: Cambridge University Press)
[106] Punning A and Jalviste E 2009 Analytical Solution for Voltage-Step Response of Lossy Distributed RC Lines *IEEE Trans. Microw. Theory Tech.* **57** 449–57
[107] Storn R and Price K 1997 Differential Evolution – A Simple and Efficient Heuristic for global Optimization over Continuous Spaces *J. Glob. Optim.* **11** 341–59
[108] Moeinkhah H, Jung J-Y, Jeon J-H, Akbarzadeh A, Rezaeepazhand J, Park K C and Oh I-K 2013 How does clamping pressure influence actuation performance of soft ionic polymer–metal composites? *Smart Mater. Struct.* **22** 025014

ACKNOWLEDGEMENTS

My sincere gratitude belongs to my supervisors Dr. Andres Punning and Prof. Alvo Aabloo for their valuable advice, guidance and for their patience during my studies. I am grateful to the supportive colleagues of Intelligent Materials and Systems Lab who have helped me to reach my goals. My special thanks are addressed to Dr. Urmas Johanson for endless constructive discussions in the field of electrochemistry. I also would like to thank Ms. Inga Põldsalu and Ms. Inna Baranova for preparing the samples, which are characterized throughout the experimental part of this dissertation. Sincere gratitude should be given to my colleague Dr. Mehmet Itik for a productive collaboration. I highly acknowledge Dr. Anna-Liisa Peikolainen for proofreading this thesis.

Last, but not least, I very much appreciate the continuous support from my wife Kersti, my daughters Anni and Eliise, my mother and father, and all other relatives. Thank you all.

This work has been financially supported by the Estonian Science Foundation grant nos. 7811, 8553, and 9216, and by Institutional Research Funding project IUT20-24 from Estonian Research Council. I acknowledge the financial support from the European Social Fund's Internationalization Programme (DoRa) and the Estonian Doctoral School in Information and Communication Technology.

PUBLICATIONS

CURRICULUM VITAE

Name:	Veiko Vunder
Date of birth:	July 28, 1986
Birth place:	Koigi, Estonia
Nationality:	Estonian
Marital status:	Married
Phone:	+372 53 424 334
E-mail:	veiko.vunder@ut.ee

Education:

Since 09/2010	**Graduate Student** in Engineering and Technology (supervisors: Dr. A. Punning, Prof. A. Aabloo)
06/2010	**Graduation as M.Sc.** on the topic *Constructing and prototyping variable focal length lens system* (supervisors: Dr. A. Punning, Prof. A. Aabloo)
09/2008-06/2010	Master student, University of Tartu (Estonia)
06/2008	**Graduation as B.Sc.** on the topic *Removal of NOx by dielectric barrier discharge and catalyst: implementation of automated control of the experiment* (supervisor: I. Jõgi)
09/2005-06/2008	Bachelor student, University of Tartu (Estonia)
06/2005	**Abitur**
09/2002-06/2005	Tarvastu Gymnasium

Industry:

11/2008-10/2010	3D Technologies R&D, software developer.

Teaching:

Since 09/2011	Teaching assistant in „*Practical Works in Computer Hardware*"
Since 09/2015	Teaching assistant in "*Computer Architecture and Hardware I*"
09/2012–06/2013	Supervised BSc thesis E. Hamburg "*The relation between bending deflection and blocking force of the ionic polymer-metal composite (IPMC) with carbonaceous electrodes*"
Since 2012	Actively contributed to educational robotics in Estonia through supervising several robotics hobby groups and participating in FIRST® LEGO® League competitions as a referee.

Publications (in addition to the six publications included in this thesis)

Peer-review

1) A. Punning, I. Must, I. Põldsalu, **V. Vunder**, R. Temmer, K. Kruusamäe, F. Kaasik, J. Torop, P. Rinne, T. Lulla, U. Johanson, T. Tamm, and A. Aabloo, "Lifetime measurements of ionic electroactive polymer actuators," J. Intell. Mater. Syst. Struct., vol. 25, no. 18, pp. 2267–2275, Aug. 2014.
2) I. Must, **V. Vunder**, F. Kaasik, I. Põldsalu, U. Johanson, A. Punning, and A. Aabloo, "Ionic liquid-based actuators working in air: The effect of ambient humidity," Sensors Actuators B Chem., vol. 202, pp. 114–122, Oct. 2014.
3) A. Punning, K. Kim, V. Palmre, F. Vidal, C. Plesse, N. Festin, A. Maziz, K. Askaka, T. Sugino, G. Alici, G. Spinks, G. Wallace, I. Must, I. Põldsalu, **V. Vunder**, R. Temmer, K. Kruusamäe, J. Torop, F. Kaasik, P. Rinne, U. Johanson, A.-L. Peikolainen, T. Tamm and A. Aabloo, "Ionic electroactive polymer artificial muscles in space applications," Scientific Reports, 4(6913), 1–6, 2014
4) **V. Vunder**, M. Itik, I. Põldsalu, A. Punning and A. Aabloo, "Inversion-based control of ionic polymer–metal composite actuators with nanoporous carbon-based electrodes," Smart Materials & Structures, 23(2), 025010, 2014

Conference proceedings

1) **V. Vunder**, A. Punning and A. Aabloo, "Long-term behavior of ionic electroactive polymer actuators in variable humidity conditions," Proc. SPIE, 90561Y, 2015
2) A. Punning, I. Must, I. Põldsalu, **V. Vunder**, F. Kaasik, R. Temmer, A. Aabloo, "Long-term degradation of the ionic electroactive polymer actuators," Proc. SPIE 94300S, 2015
3) A. Punning, I. Põldsalu, F. Kaasik, **V. Vunder**, A. Aabloo, "Micro-mechanics of ionic electroactive polymer actuators," Proc. SPIE 94301K, 2015
4) **V. Vunder**, M. Itik, A. Punning and A. Aabloo, "Force control of ionic polymer-metal composite actuators with carbon-based electrodes," Proc. SPIE 90561Y, 2014
5) **V. Vunder**, A. Punning and A. Aabloo, "Variable-focal lens using electroactive polymer actuator," Proc. SPIE, 79771E, 2011

ELULOOKIRJELDUS

Nimi:	Veiko Vunder
Sünniaeg:	28.07.1986
Sünnikoht:	Koigi, Eesti
Kodakondsus:	Eesti
Perekonnaseis:	abielus
Telefon:	+372 53 424 334
E-post:	veiko.vunder@ut.ee

Haridus:

alates 2010	**Doktorant** Tehnika ja tehnoloogia erialal (juhendajad: Dr. A. Punning, Prof. A. Aabloo)
2010	**Tehnikateaduse magister** teemal „*Fokuseeritava läätse-süsteemi konstrueerimine ja prototüüpimine*“ (juhendajad: Dr. A. Punning, Prof. A. Aabloo)
2008–2010	Magistrant, Loodus- ja tehnoloogiateaduskond, Tartu Ülikool
2008	**Tehnikateaduse bakalaureus** teemal „*NOx kõrvaldamine gaaslahenduse ja fotokatalüsaatori koosmõjul: eksperimendi arvutijuhitavaks tegemine CCD kaamera juhtprogrammi valmistamine“* (juhendaja: I. Jõgi)
2005–2008	Bakalaureant, Füüsika-keemiateaduskond, Tartu Ülikool
2002–2005	Tarvastu Gümnaasium

Teenistuskäik:

2008–2010	3D Technologies R&D, tarkvaraarendaja.

Õppetöö:

alates 2015	Juhendaja õppeaines “*Arvuti arhitektuur ja riistvara I*”
alates 2011	Juhendaja õppeaines „*Arvutiriistvara praktikum*”
2012–2013	Juhendaja E. Hamburgi bakalaureusetööle teemal “*Süsinik-elektroodidega ioonpolümeer-metall komposiitmaterjali painde ja jõu vahelise sõltuvuse uurimine“*
alates 2012	Panustanud Eesti hariduslikku robootikasse juhendades mitmeid meeskondi ja osaledes FIRST® LEGO® League võistlustel kohtunikuna.

Publikatsioonid (lisaks käesolevas doktoritöös sisalduvatele kuuele publikatsioonile):

Ajakirjaartiklid

1) A. Punning, I. Must, I. Põldsalu, **V. Vunder**, R. Temmer, K. Kruusamäe, F. Kaasik, J. Torop, P. Rinne, T. Lulla, U. Johanson, T. Tamm, and A. Aabloo, "Lifetime measurements of ionic electroactive polymer actuators," J. Intell. Mater. Syst. Struct., vol. 25, no. 18, pp. 2267–2275, Aug. 2014.
2) Must, **V. Vunder**, F. Kaasik, I. Põldsalu, U. Johanson, A. Punning, and A. Aabloo, "Ionic liquid-based actuators working in air: The effect of ambient humidity," Sensors Actuators B Chem., vol. 202, pp. 114–122, Oct. 2014.
3) Punning, K. Kim, V. Palmre, F. Vidal, C. Plesse, N. Festin, A. Maziz, K. Askaka, T. Sugino, G. Alici, G. Spinks, G. Wallace, I. Must, I. Põldsalu, **V. Vunder**, R. Temmer, K. Kruusamäe, J. Torop, F. Kaasik, P. Rinne, U. Johanson, A.-L. Peikolainen, T. Tamm and A. Aabloo, "Ionic electro-active polymer artificial muscles in space applications," Scientific Reports, 4(6913), 1 – 6, 2014
4) **V. Vunder**, M. Itik, I. Põldsalu, A. Punning and A. Aabloo, "Inversion-based control of ionic polymer–metal composite actuators with nanoporous carbon-based electrodes," Smart Materials & Structures, 23(2), 025010, 2014

Kogumikuartiklid

1) **V. Vunder**, A. Punning and A. Aabloo, "Long-term behavior of ionic electroactive polymer actuators in variable humidity conditions," Proc. SPIE, 90561Y, 2015
2) A. Punning, I. Must, I. Põldsalu, **V. Vunder**, F. Kaasik, R. Temmer, A. Aabloo, "Long-term degradation of the ionic electroactive polymer actuators," Proc. SPIE 94300S, 2015
3) A. Punning, I. Põldsalu, F. Kaasik, **V. Vunder**, A. Aabloo, "Micro-mechanics of ionic electroactive polymer actuators," Proc. SPIE 94301K, 2015
4) **V. Vunder**, M. Itik, A. Punning and A. Aabloo, "Force control of ionic polymer-metal composite actuators with carbon-based electrodes," Proc. SPIE 90561Y, 2014
5) **V. Vunder**, A. Punning and A. Aabloo, "Variable-focal lens using electro-active polymer actuator," Proc. SPIE, 79771E, 2011

DISSERTATIONES TECHNOLOGIAE UNIVERSITATIS TARTUENSIS

1. **Imre Mäger.** Characterization of cell-penetrating peptides: Assessment of cellular internalization kinetics, mechanisms and bioactivity. Tartu 2011, 132 p.
2. **Taavi Lehto.** Delivery of nucleic acids by cell-penetrating peptides: application in modulation of gene expression. Tartu 2011, 155 p.
3. **Hannes Luidalepp**. Studies on the antibiotic susceptibility of *Escherichia coli*. Tartu 2012, 111 p.
4. **Vahur Zadin**. Modelling the 3D-microbattery. Tartu 2012, 149 p.
5. **Janno Torop**. Carbide-derived carbon-based electromechanical actuators. Tartu 2012, 113 p.
6. **Julia Suhorutšenko.** Cell-penetrating peptides: cytotoxicity, immunogenicity and application for tumor targeting. Tartu 2012, 139 p.
7. **Viktoryia Shyp.** G nucleotide regulation of translational GTPases and the stringent response factor RelA. Tartu 2012, 105 p.
8. **Mardo Kõivomägi.** Studies on the substrate specificity and multisite phosphorylation mechanisms of cyclin-dependent kinase Cdk1 in *Saccharomyces cerevisiae*. Tartu, 2013, 157 p.
9. **Liis Karo-Astover.** Studies on the Semliki Forest virus replicase protein nsP1. Tartu, 2013, 113 p.
10. **Piret Arukuusk**. NickFects–novel cell-penetrating peptides. Design and uptake mechanism. Tartu, 2013, 124 p.
11. **Piret Villo.** Synthesis of acetogenin analogues. Asymmetric transfer hydrogenation coupled with dynamic kinetic resolution of α-amido-β-keto esters. Tartu, 2013, 151 p.
12. **Villu Kasari.** Bacterial toxin-antitoxin systems: transcriptional cross-activation and characterization of a novel *mqsRA* system. Tartu, 2013, 108 p.
13. **Margus Varjak.** Functional analysis of viral and host components of alphavirus replicase complexes. Tartu, 2013, 151 p.
14. **Liane Viru.** Development and analysis of novel alphavirus-based multifunctional gene therapy and expression systems. Tartu, 2013, 113 p.
15. **Kent Langel.** Cell-penetrating peptide mechanism studies: from peptides to cargo delivery. Tartu, 2014, 115 p.
16. **Rauno Temmer**. Electrochemistry and novel applications of chemically synthesized conductive polymer electrodes. Tartu, 2014, 206 p.
17. **Indrek Must.** Ionic and capacitive electroactive laminates with carbonaceous electrodes as sensors and energy harvesters. Tartu, 2014, 133 p.
18. **Veiko Voolaid.** Aquatic environment: primary reservoir, link, or sink of antibiotic resistance? Tartu, 2014, 79 p.

19. **Kristiina Laanemets.** The role of SLAC1 anion channel and its upstream regulators in stomatal opening and closure of *Arabidopsis thaliana.* Tartu, 2015, 115 p.
20. **Kalle Pärn**. Studies on inducible alphavirus-based antitumour strategy mediated by site-specific delivery with activatable cell-penetrating peptides. Tartu, 2015, 139 p.
21. **Anastasia Selyutina.** When biologist meets chemist: a search for HIV-1 inhibitors. Tartu, 2015, 172 p.
22. **Sirle Saul**. Towards understanding the neurovirulence of Semliki Forest virus. Tartu, 2015, 136 p.
23. **Marit Orav**. Study of the initial amplification of the human papillomavirus genome. Tartu, 2015, 132 p.
24. **Tormi Reinson.** Studies on the Genome Replication of Human Papillomaviruses. Tartu, 2016, 110 p.
25. **Mart Ustav Jr.** Molecular Studies of HPV-18 Genome Segregation and Stable Replication. Tartu, 2016, 152 p.
26. **Margit Mutso**. Different Approaches to Counteracting Hepatitis C Virus and Chikungunya Virus Infections. Tartu, 2016, 184 p.
27. **Jelizaveta Geimanen**. Study of the Papillomavirus Genome Replication and Segregation. Tartu, 2016, 168 p.
28. **Mart Toots**. Novel Means to Target Human Papillomavirus Infection. Tartu, 2016, 173 p.
29. **Kadi-Liis Veiman.** Development of cell-penetrating peptides for gene delivery: from transfection in cell cultures to induction of gene expression *in vivo*. Tartu, 2016, 136 p.
30. **Ly Pärnaste**. How, why, what and where: Mechanisms behind CPP/cargo nanocomplexes. Tartu, 2016, 147 p.
31. **Age Utt**. Role of alphavirus replicase in viral RNA synthesis, virus-induced cytotoxicity and recognition of viral infections in host cells. Tartu, 2016, 183 p.